

# Yarkovsky/YORP chronology of young asteroid families

D. Vokrouhlický and M. Brož

*Institute of Astronomy, Charles University, V Holešovičkách 2, 18000 Prague 8, Czech Republic*

W.F. Bottke and D. Nesvorný

*Southwest Research Institute, 1050 Walnut St, Suite 400, Boulder, CO 80302, USA*

A. Morbidelli

*Observatoire de la Côte d’Azur, BP 4229, 06304 Nice Cedex 4, France*

## ABSTRACT

Most asteroid families are outcomes of unique disruption events that have happened in the main asteroid belt in the past. Except for the case of two very young families, Karin and Veritas, we currently miss accurate enough information about their age. Yet, this information is critical in using data of the observed families for various planetary-science interpretations such as inferences about the initial velocity fields after the parent-body breakup, space weathering processes, etc. In this paper we develop a method that allows us to estimate ages of young asteroid families (if they are approximately in between 0.1 and 1 Gy). We apply it to four suitable cases – Erigone, Massalia, Merxia and Astrid – and discuss obstacles that prevent using our method to other ones. Together with Veritas family, they seem to be outcomes of all large disruptions (i.e. parent body  $\geq 100$  km) that have happened in the main asteroid belt in the past  $\sim 0.75$  Gy. We confirm that asteroid families are undergoing dynamical evolution due to thermal forces and torques.

*Subject headings:* asteroids, asteroid families, Yarkovsky effect

## 1. Introduction

Asteroid families have been receiving a considerable attention during the past decades (e.g. Bendjoya and Zappalà, 2002; Cellino et al., 2002; Zappalà et al., 2002). Unlike a random sample of asteroids across the main belt, the asteroids in families possess a unique quality of being “genetically linked” to a collisional break-up of the common parent body at a particular common time. The relation to a single parent object offers a possibility to study its mineralogical structure via analysis of homogeneity or heterogeneity of the surface properties of family members, available through spectroscopic observations. The relation to the single parent event brings a possibility to study the outcomes of disruptions of large bodies, otherwise laboratorily inaccessible, such as

the resulting velocity field and size distribution of the created fragments. Also counting the observed families should advice us about the number of disruptions of large bodies in the main asteroid belt, and constrain thus the overall collisional history of minor bodies in between Mars and Jupiter.

Since no good science problem is simple, the listed goals have their own difficulties to be faced. For instance, spectral properties of currently observed family members might not directly hint us about the mineralogical properties of the parent object because space weathering processes might have operated over the age of the family to diverge them (e.g. Chapman, 2004; Jedicke et al., 2004; Nesvorný et al., 2005). The family might have also been created in a populous asteroid zone, so that a number of interloper bodies would drive unrealistic spectral dissimilarities (e.g. Miglior-

ini et al., 1995). Similarly, we likely do not observe today the configuration of the family members as frozen from time they have been created as collisional fragments from the parent event. Their cluster has undergone collisional grinding, being hit by background-population projectiles, thus the observed size distribution of the family members likely adapted to the overall background-population size distribution starting from the small-sizes end. At the same time, both gravitational and non-gravitational perturbations work together to modify orbital configuration of the family members (e.g. Bottke et al., 2001, 2002; Nesvorný et al., 2002a). In this way, today’s family clusters may largely hide information on the initial velocity field with which the fragments have been initially distributed relative to each other. Finally, a simple counting of today’s families could provide misleading information about total number of families created in the past if not corrected by the fact that small clusters disperse due to the mentioned collisional effects and orbital perturbations and become unrecognized in the background population of asteroids (e.g. Marzari et al., 1999).

An underlying fundamental issue to many of the potential problems mentioned above is that we observe the asteroid families today, after an a priori unknown timespan of collisional and dynamical evolution has elapsed since their creation. Determining the ages of the asteroid families thus comes as a critical topic.

A number of methods have been proposed to deal with the asteroid family age-problem (e.g. Nesvorný et al., 2005 or Vokrouhlický et al., 2005 and references therein.). Having revised the principal possible evolutionary alterations, many of which depend on not well constrained parameters, one understands that dating young families is a more simple task than dating old families. By a matter of principle, young families are expected to be statistically smaller and we had to wait until a large number of asteroid orbits are known, and determined well-enough to compute their proper elements, in order to identify these small clusters (e.g. Milani and Knežević, 2000; Knežević and Milani, 2003; Knežević et al., 2002). An unprecedented leap forward has been performed in this respect over the past decade, both due to modern observational programs and computational efforts (<http://newton.dm.unipi.it/>). Thus Nesvorný

et al. (2002b, 2003) achieved the most accurate to-date age determination of the Karin cluster –  $5.75 \pm 0.05$  My – using direct propagation of the asteroid orbits backward in time (see also Nesvorný and Bottke, 2004). This method has been also successfully applied to the Veritas family –  $8.3 \pm 0.5$  My old (Nesvorný et al., 2003) – crowning thus efforts since Milani and Farinella (1994) suggested using chaotic chronology a young age for this cluster. Unfortunately, the direct method is limited to families younger than about 10 My or even inapplicable at all if the underlying zone is highly chaotic (such as the case of the Iannini family, Nesvorný et al., 2003). Beyond this age quite less accurate methods must be applied.<sup>1</sup>

Binzel (1987, 1988) analyzed distribution of the asteroid rotation rates in the Eos and Koronis families. Differences among the two cases, a relaxed Maxwellian distribution for the Eos family and irregular distribution with systematically longer rotation periods for the Koronis family, let this author conclude that Eos family must be comparably much older than the Koronis family. An age comparable to the Solar System lifetime was thus inferred for Eos, while Koronis was suggested considerably younger. A more recent studies though indicate drawbacks in this method. Vokrouhlický et al. (2005) confirm the Eos family is  $\sim 1.3$  Gy old. More surprisingly, though, Bottke et al. (2001) conclude an even larger age for the Koronis family –  $\sim 2 - 3$  Gy – to allow populating the Prometheus clan by multikilometre asteroids. Slivan (2002), Slivan and Binzel (1996) and Slivan et al. (2003) then brought a new light into Koronis members rotation rate distribution, showing its bimodal nature with a fast- and slow-rotating populations. Finally, Vokrouhlický et al. (2003) matched the puzzling rotation rate and obliquity distribution using a model where the initially random distribution is affected on a long-

---

<sup>1</sup>A “less-ambitious variant” of the direct backward integration of orbits has been originally proposed by Brouwer (1951) who noted that the sum of proper longitude of ascending node  $\Omega_p$  and proper longitude of pericenter  $\varpi_p$  is stationary in the linearized perturbation theory. Any clustering in this sum, presumably only slowly dispersing due to higher-order perturbation terms, was seen as a signature of the family’s young age. Brouwer (1951) thus argued for the young age of the Eos family, but a critical reassessment of the argument by Farinella et al. (1989) and lately by Vokrouhlický et al. (2005) showed caveats of this method.

term by thermal torques (also discussed below). Not only this was the first hint that these thermal torques, related to the thermal (Yarkovsky) forces, efficiently operate on multikilometre asteroids but also their model requires the Koronis age be larger than  $\sim 2.5$  Gy, in accord with orbital inferences, collisional grinding model and cratering record on Ida.

Another possibility to estimate ages of the asteroid families is to analyse their size distribution and compare it with a simulation (e.g. Marzari et al., 1995, 1996, 1999). As an example, Marzari et al. (1995) had a moderate success in fitting the size distribution of the Koronis and Themis asteroid populations while for both determining an age exceeding  $\sim 2$  Gy. For the Eos family, though, they have not been able to find a reasonable solution. Potential caveats of this method are: (i) the unknown initial size distribution in the family (related to the unknown sizes of the parent object and projectile that caused it disrupt) and (ii) a number of free parameters in modelling the subsequent collisional evolution of family asteroids (such as their strength with respect to the catastrophic disruption as a function of size, etc.). These many unknown factors can produce biased answers, or at best correlated age determinations with some of the other solved-for parameters.

A particular possibility to hint about the family age is to use a spacecraft observation of some of its members. Crater counting on its surface, together with a model of size distribution for the impactor population, can constrain the age of the terrain. Assuming the body is primordial in the family, the same information constrains the family age. This method has been applied to the asteroid (951) Gaspra, a  $\sim 6$  km member of the Flora family, and (243) Ida, a  $\sim 15$  km member of the Koronis family. In the Gaspra’s case, the best determination of the surface age ranges between 200 and 500 My (e.g. Chapman et al., 1996; Chapman, 2003). This age for Flora family coincides with the dispersal time of any compact cluster in this particular region of the main asteroid belt by chaos related to weak resonances (e.g. Nesvorný et al., 2002a). Such age makes also good sense provided the Flora family event coincides with formation of the L chondrite meteorites, that are isotopically dated to  $\sim 500$  My (e.g. Haack et al., 1996). Similarly, the age of Ida from its cratering record –

some 2 Gy – matches independent determinations of the Koronis family age mentioned above.

Finally, Farinella and Vokrouhlický (1999) brought the idea of using family dispersion by the Yarkovsky forces to estimate its age. For instance Vokrouhlický et al. (2002) estimated the age of the Eos family to  $\sim 2$  Gy. Nesvorný et al. (2003, 2005) and Carruba et al., (2003) used the same method to estimate ages of several other asteroid families. While pointing a good principle, these works represent an infancy of the method. For instance, no room was given in these attempts to the role of the initial velocity-field scatter of the asteroids and this is a reason why Vokrouhlický et al. (2005), applying the method introduced here, have recently refined the estimate of the Eos family age to  $1.3^{+0.15}_{-0.2}$  Gy.

The purpose of this paper is to bring the Yarkovsky chronology of the asteroid families to a higher level of sophistication. By involving “the other face of thermal phenomena”, namely thermal torques affecting asteroids’ rotation, we overcome the apparent impasse of not being able to decorrelate the effects of Yarkovsky dispersion of the family and its initial velocity dispersion. This is a major achievement in this paper. We show that our selected families had an initial semimajor axis extension equivalent to about 30 – 50% of the currently observed family. The remaining part has been acquired later as a result of the dynamical dispersion due to the Yarkovsky forces. This result is in a good agreement with an independent analysis of Dell’Oro et al. (2004), who suggest that the initial families were smaller than the observed families by a factor of two. Our work, though, also allows us to approximately determine the age of the respective family.

Sec. 2 is devoted to introduce in detail our method. In Secs. 3 and 4 we apply this new method to a selected families; first we characterize them anew as clusters in the proper element space using their most up-to-date catalogue and then we determine their ages. In Sec. 5 we support our model by direct numerical integration of long-term orbital evolution with thermal forces for a sample of asteroids in each of our families. These results illustrate some interesting features such as interaction of migrating orbits with weak mean motion resonances. In Discussion, Sec. 6, we deal with limitations of our method and explain why it can-

not be used for all observed asteroid families.

## 2. The method

Asteroid families are usually recognized as a statistically significant clusters in the space of proper orbital elements: semimajor axis  $a$ , eccentricity  $e$  and inclination  $I$ . Various methods have been developed for this identification (e.g. Bendjoya and Zappalà, 2002). Families are born and evolve in this three-dimensional space. Additional dimension they occupy is that of sizes  $D$  of the family members, which by itself undergoes some evolution. Two principal features of the Yarkovsky forces should be recalled here: (i) they secularly affect mainly orbital semimajor axis, while to a much smaller extent the eccentricity and inclination, making thus the initial family disperse in the semimajor axis direction (e.g. Vokrouhlický, 1998; Vokrouhlický and Farinella, 1998, 1999), and (ii) they are size dependent. As a result, out of the four dimensions noted above the Yarkovsky forces make differentially expand the family in the  $(a, D)$  subspace, and perform nearly no evolution along the  $(e, I)$  directions. For this reason we neglect the information about the eccentricities and inclinations in this paper, and fold our analysis entirely to the  $(a, D)$  subspace. In fact, we replace size  $D$  with absolute magnitude  $H$ , and observationally more accessible quantity that, under assumptions, may be converted to  $D$ .

The families do evolve in  $(e, I)$  directions due to the planetary gravitational perturbations (and chaotic motion related to their resonances; e.g. Morbidelli and Nesvorný, 1998; Nesvorný and Morbidelli, 1999; Nesvorný et al., 2002a), but so in a largely uncorrelated way to their evolution in the semimajor axis direction. This holds true to a less extend for very old families, where the Yarkovsky migrating orbits might be trapped in the weak resonances and their semimajor axis changes temporarily halted, but it is a very good assumption for a rather young families that are of concern in this paper. Because of their youth, we shall also neglect in this work the effects of collisional grinding in sizes of the family members.

A typical asteroidal family exhibits a characteristic pattern when its members are projected onto the plane defined by semimajor axis  $a$  and absolute magnitude  $H$ : the largest asteroid resides near the

mean value of  $a$  for the whole family, while the extreme values of  $a$  are occupied by the smallest asteroids only. Because it appears natural that smaller fragments received larger relative velocity with respect to the parent body during the initial catastrophic disruption, Cellino et al. (1999) attempted to use this distribution of family members to calibrate the unknown velocity-size relation assuming families did not dynamically evolve in semimajor axes since their formation. (This work followed an earlier study by Zappalà et al. (1996), except for recognizing that proper  $e$  and  $I$  might be unstable on a long-term due to effects of weak resonances; Cellino et al. (1999) thus decided to use the proper semimajor axis only.) Hereafter we go on along arguing that even this element should be abandoned for their task due to perturbation by the thermal effects. In order to strengthen our arguments and results we, however, find useful to contrast our more general model with this simplified approach (Sec. 2.2).

### 2.1. General considerations

Let us start with general considerations and proceed then from simple toward more general models. Consider a projection of the family members onto the  $(a, H)$  plane. In general, the result is a clump of data points. A model whose ambition is to interpret the family, such as the initial velocity field or Yarkovsky dispersal scenario, necessarily entails some parametric relation between  $H$  and  $a$ , say  $H = H(a; p_1, p_2, \dots)$ , where  $(p_1, p_2, \dots)$  are some parameters. When this functional representation is a one-to-one mapping, that can be for instance achieved by fixing all but one parameter  $p_n$  say, we can characterize the family with distribution function  $\mathcal{D}(p_n)$  of this parameter in some interval of  $p_n$  values:

$$\mathcal{D}(p_n) = \frac{dN}{dp_n}, \quad (1)$$

where  $dN$  is number of family asteroids in the  $(a, H)$ -strip generated by changing  $p_n$  in the range  $(p_n, p_n + dp_n)$ . Function  $\mathcal{D}(p_n)$  then contains entire information about the family within this model.

The most general, yet still very simple, parametric relation we shall consider in this paper is given by

$$0.2 \beta H = \log(\Delta a / C), \quad (2)$$

with  $\Delta a = a - a_c$ ; we argue in Sec. 2.3 that this form is tailored to the Yarkovsky dispersion model. Equation (2) gives  $H$  a function of  $a$  using three parameters  $H = H(a; \beta, a_c, C)$ : (i)  $\beta$  positive, (ii)  $a_c$  basically shifts the origin in  $a$ , and (iii)  $C$  can acquire both negative and positive values in some interval. In our application below we always fix  $\beta$  and  $a_c$ , considering thus density function  $\mathcal{D}(C)$  of the last parameter  $C$ .

## 2.2. A toy model # 1: Initial dispersion of fragments

Let us start with a simple, unrealistic model of a family represented by the initial distribution of ejecta from disruption of a parent body. Assuming the latter reside on near-circular orbit with semi-major axis  $a_c$ , thus neglecting eccentricity corrections in the following equations, a fragment ejected with a transverse velocity  $V_T$  is thrown onto an orbit with semimajor axis difference

$$\Delta a = \frac{2}{n} V_T + \mathcal{O}(e) \quad (3)$$

with respect the orbit of the parent body (i.e.  $\Delta a = a - a_c$  as above). Here  $n$  is the heliocentric mean motion of the parent body. Next we assume

$$V_T = V_0 \left( \frac{D_0}{D} \right)^\beta \cos \alpha, \quad (4)$$

where  $D$  is the size of the body,  $D_0$  and  $V_0$  are some reference values and  $\alpha$  is directional cosine of the fragment's velocity with respect the transverse direction to the parent body orbit.<sup>2</sup> The velocity  $V_0$  and the (positive) exponent  $\beta$  are a priori unknown parameters. Data from the young Karin cluster are consistent with  $\beta \simeq 1$  (Nesvorný et al. 2002), while several papers considered analytical arguments in favor of particular  $\beta$  value (such that  $\beta \simeq 3/2$  in Cellino et al., 1999). The Eq. (4) is highly idealized since it assumes that bodies of size  $D$  were all ejected with the same velocity  $V_0 (D_0/D)^\beta$ . Let us stay for a while with this assumption and recall the generic relation  $D = D_0 10^{-0.2H} / \sqrt{p_V}$  between the absolute magnitude  $H$  and size  $D$  (e.g. REF?):  $D_0 = 1329$  km,

<sup>2</sup>In fact the velocity field of fragments should be related to the center of mass frame of the parent body and the projectile that causes its disruption but here we neglect this correction for simplicity; the relevant formulas can be found e.g. in Marzari et al. (1995).

is going to be the reference size value introduced above, and  $p_V$  is geometric albedo in optical band. Assuming  $p_V$  is size-independent, the family members are distributed in the  $(a, H)$  space according to Eq. (2) with

$$C = \frac{2}{n} V_0 p_V^{\beta/2} \cos \alpha = C_0 \cos \alpha. \quad (5)$$

The most simple, though often invoked, assumption is the isotropy of fragment ejection in space. In this model  $\cos \alpha$  is uniformly distributed in the interval  $(-1, 1)$  and thus  $C$  acquires uniform values between  $-C_0$  and  $C_0$ . For the same reason, the density function  $\mathcal{D}(C)$  is constant (note we write  $\mathcal{D}(C) = dN/dC = (dN/d \cos \alpha) (d \cos \alpha/dC)$  and each of these two multiplicative factors is constant). Simplicity of this result indicates the functional relation  $H(a)$  as in Eq. (2) is well suited (optimized) for this model.

Perhaps the most restrictive assumption above is that of constant ejection velocity for fragments of a given size  $D$ . There is certainly some dispersion of velocity even for fragments of the same size  $D$  and this would make the previous analysis more complicated. An example of modeling this effect is a work by Petit and Farinella (1993), who give the transverse velocity  $V_T$  as a Gaussian function with the half-width parametrically depending on size of the fragment. In this case the template relation (2) is no more tailored to the model, yet we point out it can still be formally used and it still have a good sense to define the density function  $\mathcal{D}(C)$  of the formal parameter  $C$ . We find numerically, that within this model  $\mathcal{D}(C)$  is no more constant on a finite interval of values, but it has a maximum for  $C = 0$  and drops to zero when  $|C| \rightarrow \infty$ . Similarly, if the initial velocity is not isotropic but contains a preferred direction,  $\cos \alpha$  is not uniform and this produces variations in  $\mathcal{D}(C)$ . This is often seen in output of numerical simulations (e.g. Love and Ahrens, 1996; Ryan and Melosh, 1998; Benz and Asphaug, 1999; Michel et al., 2001, 2002) and also supported by analysis of young clusters like Karin or Veritas.

## 2.3. A toy model # 2: Yarkovsky diffusion

Our second toy model illustrates basic features of the Yarkovsky dispersion scenario. Now we assume all family asteroids have the same initial value of the semimajor axis  $a_c$  with their initial

spin axes randomly oriented in space and kept fixed in time. Alike initially assigning the same value of the semimajor axis to all fragments, this last assumption is also certainly not true, because a number of dynamical effects (such as thermal and gravitational torques) and collisional tugs are permanently moving spin axis and changing rotation rate.

Because of the Yarkovsky forces, each asteroid would have in time  $T$  a new value of the semimajor axis  $a = a_c + (da/dt) T$ , where  $da/dt$  is the rate of change in semimajor axis. For asteroids larger than  $\simeq 50$  metres, and any reasonable thermal properties of their surfaces,  $(da/dt) \propto D^{-1}$  for the size  $D$  (e.g. Bottke et al., 2002). Moreover, the diurnal variant of the Yarkovsky effect is likely to dominate  $(da/dt)$  over the seasonal variant by at least an order of magnitude. Denoting spin axis obliquity  $\epsilon$ , we have  $(da/dt) \propto \cos \epsilon$  (thus  $|\kappa_1| \gg |\kappa_2|$  in Eq. (8)). Choosing an arbitrary reference size  $D_0$ , we thus have a two-parametric dependence of  $(da/dt)$  such that  $(da/dt) = (da/dt)_0 (D_0/D) \cos \epsilon$ , with  $(da/dt)_0$  a maximum Yarkovsky rate of change of the semimajor axis for a body of size  $D_0$  (with zero obliquity). For convenience  $D_0 = 1329$  km as above. Assuming finally that all asteroids have the same value of the surface geometric albedo  $p_V$  in optical, each of them would in time  $T$  reach a point  $(a, H)$  so that

$$0.2 H = \log (\Delta a / C) , \quad (6)$$

with  $\Delta a = a - a_c$  and

$$C = \sqrt{p_V} (da/dt)_0 T \cos \epsilon = C_0 \cos \epsilon . \quad (7)$$

Note Eq. (6) has again the same functional form as in Eq. (2) with  $\beta = 1$ , a direct consequence of the size dependence of  $da/dt$ . In our model  $\cos \epsilon$  has a uniform distribution in the interval  $(-1, 1)$ , thus again  $C$  acquires uniformly values in the interval  $(-C_0, C_0)$ . It also follows that  $\mathcal{D}(C)$  is constant on the same interval of values. With  $p_V$  fixed, the limiting values  $C_0$  directly constrain age  $T$  of the family. This simple representation has been used earlier by Vokrouhlický et al. (2002) and later by Nesvorný et al. (2003, 2005) to estimate the age of Eos and several other families.

## 2.4. Toward a more general model

To a large degree, both toy models from Secs. 2.2 and 2.3 yield very similar results: when  $\beta \simeq 1$ , as supported by the Karin data, and a moderate dispersion in characteristic velocity with which fragments of a given size are ejected, both predict nearly constant  $\mathcal{D}(C)$  distribution function. Luckily, real families are more complex and their particular properties, producing characteristic features in the distribution function  $\mathcal{D}(C)$ , allow to discriminate between the two toy approaches. Hereafter, we demonstrate such a distinct feature in the case of our selected families, while the Eos family has been similarly analysed by Vokrouhlický et al. (2005).

Let us start, for illustration, with the Erigone family whose  $\mathcal{D}(C)$  is shown in Fig. 1. In fact we show here directly number  $N_{\text{obs}}(C)$  of Erigone members in the interval  $(C, C + \Delta C)$  values with  $\Delta C = 2 \times 10^{-6}$  AU, which is up to a scaling by  $\Delta C$  identical to  $\mathcal{D}(C)$ . An outstanding feature of this distribution, incompatible neither with the first nor with the second toy models above, are significant maxima at  $C \simeq \pm 1.5 \times 10^{-5}$  AU symmetric about the origin. The value  $\mathcal{D}(0)$  represents only about 25% of the maximum value at a very high statistical level (we use  $\sqrt{N_{\text{obs}}(C)}$  as quasi-errors of the values  $N_{\text{obs}}(C)$  in each of the bin in  $C$ ).

Such maxima in  $\mathcal{D}(C)$  misplaced from origin are a direct consequence of the fact that small asteroids tend to preferentially populate regions at the outskirts of the family and leave its center underpopulated (see the  $(a, H)$  projection, Fig. 4, for Erigone). Such a distorted distribution of family members is hard to reconcile with any reasonable ejection field of fragments in the family-forming disruption event. In particular, it would mean two anti-aligned streams of fragments are thrown to preferentially populate extremal values of  $V_T$ . Such a geometry has never been observed in numerical simulations nor it would be expected from heuristic arguments. On the other hand, the Yarkovsky dispersal model offers a natural explanation for this feature. Some may argue that the central depletion in the family is due to dispersal effect of the weak resonances, but this does not hold true as we prove later in this paper (Sec. 5.1).

In order to see the argument we need to

briefly recall basic facts about the Yarkovsky-Öpik-Radzievskii-Paddack (YORP) effect (e.g. Rubincam, 2000; Vokrouhlický and Čapek, 2002; Bottke et al., 2002). YORP is only a different face of the same thermal phenomenon that causes Yarkovsky force to affect orbital motion, since YORP means thermal torque that affects rotation of irregularly-shaped bodies. On a long term, YORP has been found to preferentially tilt obliquity toward extreme values of  $0^\circ$  and  $180^\circ$  (Čapek and Vokrouhlický, 2004) while near these asymptotic obliquity states the rotation rate is either accelerated or decelerated. This simple picture of the long-term evolution of the rotation state may be temporarily altered by spin-orbit secular resonances, such as evidenced by the Koronis family members (e.g. Vokrouhlický et al., 2003). In the same way, YORP asymptotic evolution is poorly understood today, since a steady deceleration of an asteroid’s rotation rate should result either in onset of the tumbling or drain enough angular momentum so that collisions would efficiently establish again a nominal rotation state; fast rotating asteroid then should reach at some moment a threshold of rotational fission, unless shape changes cause YORP to become decelerating the body again or become weakened. None of these details are known accurately enough so that we could easily accommodate them in our analysis and we shall thus neglect them at this moment.

The principal effect of YORP in our context is its ability to preferentially tilt obliquity toward extreme values that, in turn, help the Yarkovsky forces to affect more the orbital semimajor axis (remember the diurnal variant is likely to dominate for our bodies). With that conclusion, we would actually expect small family asteroids occupy extreme borders of the family in semimajor axis, leaving its center depleted after some time of evolution.

To test this hypothesis we constructed a simple numerical model with the goal to quantitatively match the observed  $\mathcal{D}(C)$  distribution. Its main features and parameters are as follows:

- We set initial distribution of fragments in the proper element space due to finite (non-zero) velocity field arising from the parent-body disruption. To keep things simple, we assume all velocity components  $V_R$ ,  $V_T$  and

$V_N$  along the radial, transverse and normal directions with respect to the parent body orbit have the same Gaussian distribution with standard deviation  $V_{SD}$ . We also assume  $V_{SD} = V$  ( $5 \text{ km}/D$ ) is inversely proportional to size  $D$  (thus  $\beta = 1$ ) and  $V$  is a free parameter of the model (and has values several tens of m/s). This model fits the data from the Karin family (e.g. Nesvorný et al., 2002, 2003). The number of fragments used in our simulations is the same as the number of observed asteroids in the family and we assign them the same value of absolute magnitude. This is converted to size  $D$  using the standard transformation mentioned above and we use a constant geometric albedo of  $p_V$ . As a hint for the appropriate  $p_V$  value we use data determined by Tedesco et al. (2002) from IRAS observations. In general these values are conformal to those expected from the spectral type of the family. However, to test robustness of our solution on variations in  $p_V$  we also perform several simulations with different values of this parameter.

- Apart from the size and the initial orbital elements (semimajor axis in particular), we assigned the asteroids some initial value of obliquity  $\epsilon$  and angular velocity  $\omega$  of rotation in our simulations. The initial orientation of spin axes is random in space, thus  $\cos \epsilon$  is uniformly distributed in the interval  $(-1, 1)$ , while  $\omega$  is assumed to have Gaussian distribution peaked at  $\simeq 6$  hr period. Values smaller than 2 hr and longer than 12 hr are rejected.
- Orbital evolution of each of the fragments is tracked individually. The semimajor axis  $a$  is assumed to undergo a steady change due to the Yarkovsky forces with a drift rate estimated by (e.g. Vokrouhlický, 1998, 1999)

$$\frac{da}{dt} = \kappa_1 \cos \epsilon + \kappa_2 \sin^2 \epsilon, \quad (8)$$

where  $\kappa_1$  and  $\kappa_2$  are functions depending on surface thermal parameters and the size. We use the following thermal parameters: thermal conductivity  $K = 0.005 - 0.05 \text{ W/m/K}$ , specific heat capacity  $C_p = 680 \text{ J/kg/K}$ , surface and bulk densities 2 and  $2.5 \text{ g/cm}^3$ .

Lower values of the thermal conductivity are a priori preferred for the S-type families, higher values for the C-type families, but we again check robustness of the solution by changing  $K$  in some limited interval of values. The Eq. (8) assumes (i) a spherical body residing on circular orbit about the Sun, and (ii) a restricted, linearized analysis of the heat diffusion in the asteroid's surface. Nevertheless, we find it sufficient for the purpose of our work, because tests against the complete numerical analysis show that Eq. (8) typically fails no more than by a factor 2.

- We also assume the two parameters of the rotation state, obliquity  $\epsilon$  and rotation rate  $\omega$ , undergo evolution due to the YORP effect. To model it we use

$$\frac{d\omega}{dt} = f(\epsilon), \quad (9)$$

$$\frac{d\epsilon}{dt} = \frac{g(\epsilon)}{\omega} \quad (10)$$

(e.g. Vokrouhlický and Čapek, 2002; Čapek and Vokrouhlický, 2004). The  $f$ - and  $g$ -functions here are the median strength of the YORP torques derived by Čapek and Vokrouhlický (2004) for asteroids with a surface thermal conductivity in the above stated range. Nevertheless, we suppose modeling of the YORP effect is less certain than the Yarkovsky effect. For that purpose we introduce a free parameter  $c_{\text{YORP}}$  by which we multiply  $f$ - and  $g$ -functions in Eqs. (9) and (10).

- Finally, our model contains a very simple implementation of the collisional dynamics; this is mainly because the Yarkovsky and YORP effects depend sensitively on the rotation state, which is itself dependent on collisions between asteroids. We neglect disruptive collisions, but include sub-critical collisions able to significantly re-orient spin axis of the body. An appropriate approach for this concept has been developed by Farinella et al. (1998) who obtained the following formula for the typical re-orientation timescale:

$$\tau_{\text{reor}} = B (\omega/\omega_0)^{\beta_1} (D/D_0)^{\beta_2}, \quad (11)$$

with  $B = 84.5$  ky,  $\beta_1 = 5/6$  and  $\beta_2 = 4/3$ , and the reference size  $D_0 = 2$  m and rotation frequency  $\omega_0$  corresponding to the rotation period of 5 hr. Propagating evolution of the family with timesteps  $\Delta t$ , we each time consider a probability  $\sim \Delta t/\tau_{\text{reor}}$  that the spin axis was collisionally reset to an initial random state.

With a given initial configuration of the family, we run the our code for a time  $T$ , ranging typically from 0 – 1 Gy, and we let the family evolve by the thermal effects. As mentioned above, apart from  $T$  we consider another two free-to-fit parameters:  $V$  and  $c_{\text{YORP}}$ . To obtain a measure of a quantitative agreement between the simulation and the observed Eos family, we define a pseudo- $\chi^2$  target function

$$\Psi_{\Delta C} = \sum_{\Delta C} \left( \frac{N(C) - N_{\text{obs}}(C)}{N_{\text{obs}}(C)} \right)^2, \quad (12)$$

where formally the errors assigned to the number  $N_{\text{obs}}(C)$  in a given bin  $(C, C + \Delta C)$  is  $\sqrt{N_{\text{obs}}(C)}$ . Our procedure seeks to minimize  $\Psi_{\Delta C}$  via variation of the three parameters in certain interval of values. Admissible solutions are characterized by  $\Psi_{\Delta C}$  of the order equal to the number of used bins in  $C$ , while solutions giving much larger  $\Psi_{\Delta C}$  are incompatible with the observed family.

We also note that in all solutions presented in this paper we use constant, and to-date, luminosity  $L$  of the Sun. Evolutionary models of the solar interior imply the Sun should have been about 25% fainter some 4 Gy ago (e.g. Bahcall et al., 2001; Table II). Smaller radiation flux in the past should produce weaker thermal effects, both the Yarkovsky force and YORP torque. This effect has been investigated in some depth and found small by Vokrouhlický et al. (2005) in the case of the Eos family (making this family age larger by some  $\sim 4\%$  only). Since the families we analyse in this paper are  $\leq 1$  Gy old, over which the mean solar luminosity changer by  $\sim 2 - 4\%$  at most, we may safely neglect the effects of variable  $L$  here.

### 3. Selected families: HCM identification

We start with a new identification of the asteroid families selected in this work and we postpone discussion why other families have been discarded from our sample to Sec. 6. We note that

the case of the Eos family, to which our method is also successfully applicable, has been reported by Vokrouhlický et al. (2005).

We apply hierarchical clustering method (HCM; e.g. Bendjoya and Zappalà, 2002 and references therein) to identify members of the asteroid families as tight clouds of asteroids in the space of proper elements.<sup>3</sup> We use analytically determined proper elements of nearly 170,000 main belt numbered and multi-opposition asteroids from AstDyS database (<http://newton.dm.unipi.it/>) as of November 2004. We adopt the “standard metric” of Zappalà et al. (1990, 1995) to define relative velocity of two orbits and proceed family identification with some cut-off value  $V_c$ . The tested  $V_c$  typically range an interval of 20 – 110 m/s, beyond which all known orbits in a given zone of the asteroid belt communicate (the lower range of  $\sim 20$  m/s approximately corresponds to the uncertainty of the analytic proper elements). To choose the “right” value of  $V_c$  for a given family is a matter of experimentation, upon which we shall comment in each of the cases.

Figure 2 shows all four nominal families in the usual two-dimensional projections of the proper element space, together with the background population of asteroids and other families (dots), not selected here. Principal mean motion resonances (J3/1, J5/2 and J8/3) with Jupiter and some of the relevant weaker mean motion resonances (such as J11/4, exterior resonance with Mars M1/2, three-body resonances 4J–2S–1 and 3J–1S–1 following notation of Morbidelli and Nesvorný, 1998, and Nesvorný and Morbidelli, 1999) are also shown.

### 3.1. Erigone

Figure 3, upper panel, shows the number of asteroids associated with the Erigone family as a function of the HCM velocity cutoff  $V_c$ . We note two important transitions occur along this line: (i) below  $V_c = 54$  m/s the cluster contains only few objects in an immediate surrounding of the asteroid (163) Erigone, (ii) while for  $V_c \geq 80$  m/s a whole local region of the asteroid belt coalesces with the family. The Erigone family is thus reasonably defined for cutoff velocities in between these

two critical values. In this range it only slowly accumulates additional members, presumably a fraction of outlier asteroids for larger  $V_c$  values. We thus decided to consider  $V_c = 56$  m/s as a defining value for our “nominal” Erigone family.

Cumulative distribution of absolute magnitude values  $H$  for family members can be piecewise approximated with a power-law:  $N(< H) \propto 10^{\gamma H}$ . We find it interesting to fit the magnitude range (13.5, 15.5) with that assumption. The bottom part in Fig. 3 shows the values of  $\gamma$  as a function of  $V_c$ . Interestingly, for the family defining values of  $V_c$ ,  $\gamma$  consistently oscillates between 0.74 and 0.8, giving a value  $\gamma = 0.75 \pm 0.04$  for the nominal family (see also Fig. 12 where the cumulative distributions in absolute magnitude for all our nominal families is shown). This rather steep value drops to  $\gamma \simeq 0.6$  when the background population of asteroids coalesces with the family for  $V_c \geq 80$  m/s (Fig. 3). This limiting value well coincides with the result of Ivezić et al. (2001), who give  $\gamma \simeq 0.61$  for asteroids in the absolute magnitude range (13, 15), a value perhaps dominated by the inner main-belt objects. The relative steepness of the Erigone magnitude distribution, as regards to the background, in this  $H$ -range could point toward a young age of the family, an observation that should be confirmed below.

Figure 4 shows our nominally-identified Erigone family in a various two-dimensional projections, namely proper  $e$  vs proper  $a$ , proper  $\sin I$  vs proper  $a$  and  $H$  vs proper  $a$ . The most stunning feature, common to all our families and already mentioned in Sec. 2.4, is a central depletion of the family (the best observed in the  $(a, H)$  projection). This feature cannot be attributed to any of diffusive resonances, as we check in Sec. 5.1, rather it is a consequence of the core hypothesis of our evolutionary model for the families explained in Sec. 2.4 and quantitatively developed in Sec. 4. The only relevant mean motion resonance is 4J–2S–1 that brackets the family at  $a \sim 2.41$  AU.

### 3.2. Massalia

Figure 5 shows the number of asteroids associated with the Massalia family and local power-law exponent  $\gamma$  of the cumulative magnitude distribution in the (13.5, 15.5) range as a function of the HCM velocity cutoff  $V_c$ . The critical values of  $V_c$  that bracket the reasonable family-defining

<sup>3</sup>Our program in C language is available on <http://www.boulder.swri.edu/~davidn/>.

interval are: (i) 34 m/s for which the “left side asteroids” ( $a \leq 2.405$  AU) associate with the family, and (ii) 47 m/s for which the cluster starts to accumulate a larger portion of the surrounding asteroid belt zone. In this case, we consider the value  $V_c = 44$  m/s as a suitable choice to construct our nominal realization of the Massalia family. The contrast between the family-associated  $\gamma$  value,  $\gamma = 1.03 \pm 0.03$  for the nominal family, and the overall background population is even larger than in the Erigone case. This is due to the fact, that Massalia-forming event was a cratering on a parent body with an estimated size of  $\sim 146$ – $151$  km (e.g. Tanga et al., 1999; Durda et al., 2005, in preparation). Given Massalia’s size of 145.5 km (e.g. Tedesco et al., 2002) the mass ratio of Massalia to the parent object becomes  $\sim 0.9 - 0.99$ . The second largest object in this family, thus likely the largest liberated block from the surface of the parent object, is asteroid (7760) 1990 RW3 of about 6.6 km size.<sup>4</sup> Again, at these sizes asteroid population in the main belt would be collisionally relaxed toward much a shallower size distribution unless its age is very young. Below, we again confirm this hint by placing a tight constrain on Massalia’s age.

Figure 6 shows relevant projections of our nominal Massalia family. The distribution of proper eccentricity  $e$  and inclination  $I$  have been partly affected by weak resonances, notably 4J–2S–1 and exterior M1/2 mean motion resonance with Mars. The effect of the M1/2 resonance is prominently seen in the proper inclination of Massalia’s members at  $a \sim 2.42$  AU, however this does not mean the resonance does not affect the proper eccentricity too. In fact, it does so even more and some of the former Massalia’s members might have escaped from the family while increasing or decreasing proper eccentricity (Sec. 5.2). Extremal values in semimajor axis are, as in the Erigone case, overpopulated with small asteroids. We prove below by direct numerical simulation that one cannot interpret this observation by enhanced dispersal of the centre of the family, rather it fits our scenario in which Yarkovsky and YORP effects in synergy quickly populate the extremal locations in the family.

<sup>4</sup>Note the larger associated object (2946) Muchachos is a recognized interloper in this family because of its spectral inconsistency with (20) Massalia (Monthé-Diniz et al., 2005).

### 3.3. Merxia

The number of asteroids associated with the Merxia family, and local power-law exponent  $\gamma$  of the cumulative magnitude distribution in the (13.5, 15.5) range, as a function of the HCM velocity cut-off  $V_c$  are shown in the Fig. 7. As in the Massalia family case, there are two critical values of  $V_c$ : (i) 50 m/s that brings both sides of the family together, and (ii) 108 m/s for which the family coalesces with the whole surrounding region in the main belt. In between these two values the family stays “stationary” with only little new asteroids associated. Our choice for the nominal family is  $V_c = 80$  m/s. The SFD steepness parameter  $\gamma = 0.63 \pm 0.03$  stays consistently larger than that corresponding to the local vicinity:  $\gamma \sim 0.44$  (note here we moved to the middle zone of the main asteroid belt; Fig. 2).

Figure 8, where the three characteristic projections of the Merxia family are shown, indicates very little interlopers are embedded. An outstanding exception is (1327) Namaqua with X-type classification (and anomalously low geometric albedo; see below) in contrast to the characteristic S-type classification in this family. A strong polarization of small members toward extremes in semimajor axis cannot be explained by an anomalous depletion of the central zone in the family (see below) and fits our point Yarkovsky/YORP point of view. The family is intersected by the weak 3J–1S–1 three-body resonance, but on the expected lifetime of this family it makes only a limited leakage from the family. On the other hand it directly produces the larger dispersal in proper eccentricity (and to a lesser extend inclination) for members that have been migrating toward larger values of the semimajor axis (Sec. 5.3). The family is also bracketed by the J8/3 resonance at its low- $a$  end.

### 3.4. Astrid

The Astrid family exhibits the simplest behavior as the HCM velocity cut-off  $V_c$  is being increased (Fig. 9): the number of members changes by single asteroids only up to limiting value of 133 m/s, when large portion of the middle and outer main belt zone suddenly associates with the family. Indeed, this family “lives in an isolation” with a small value of proper inclination of its members (Fig. 2). Its only evolutionary obstacle is the

nearby prominent J5/2 mean motion resonance with Jupiter, that might have perturbed asteroids reaching upper  $a$  values. A quick look at the  $(a, e)$  projection in Fig. 2 might result in a mistaken conclusion, that the zone between the Astrid family and the J5/2 resonance is populated by a number of asteroids. This is, however, not true because these apparent objects have significantly higher orbital inclination. In Fig. 10 we show a three-dimensional section of the proper elements space near the Astrid family proving that the zone in between the family and the J5/2 resonance is entirely void. We find this feature peculiar and in Sec. 5.4 we attempt to find its reason through dynamical considerations. The fact that we fail may suggest our model misses some important feature or, as we tend to believe, the initial velocity field of the Astrid family has been significantly asymmetric, populating dominantly orbits with semi-major axis smaller than that of the largest body 1128 Astrid. We note the “left side of the family” ( $a \leq 2.787$  AU) is well-determined and shows all attributes predicted by our model.

### 3.5. General issues

So far our families have been characterized in terms of the proper element clustering analysis. Our further work, though, needs additional information related to conversion of the absolute magnitudes  $H$  to sizes  $D$  for each of the asteroids. Their relation hinges upon an a priori unknown geometric albedo  $p_V$  value. To obtain, or at least constrain,  $p_V$  we use two sources.

First we note the work of Tedesco et al. (2002) who re-analysed IRAS database of infrared observations for moving objects. Geometric albedo  $p_V$  values were determined for 2228 individual objects. Among them, we searched for members of our nominal families determined above. Unfortunately, our families consist mainly of small asteroids that were not within the reach of IRAS observations. We obtained useful information mainly for Erigone and Merxia families. In the Erigone case, we identified its 6 members among the Tedesco’s et al. catalogue and all of them have albedo in the range 0.035 – 0.07, with a mean of 0.053. This value fits very well an average albedo found for the C-type asteroids. In spite of only two Merxia-family objects have albedo determined, (808) Merxia with  $p_V = 0.22 \pm 0.04$  and

(1327) Namaqua with  $p_V = 0.04 \pm 0.01$ , the information is very useful to suggest Namaqua is a interloper in the family; indeed, its spectral classification X is alien in the S-type Merxia family (Monthé-Diniz et al., 2005). Its  $p_V$  value is anomalous among the prevalent S-type bodies in this family (and anomalous as regards to the Merxia’s value) and also we have pointed out position of this asteroid in Fig. 8 showing its anomalous position in the  $(a, H)$  plane. For Massalia family we have information only about the largest body (20) Massalia with  $p_V = 0.21 \pm 0.01$ , and for the Astrid family we have (1128) Astrid with  $p_V = 0.077 \pm 0.010$  and (2169) Taiwan with  $p_V = 0.099 \pm 0.020$ . In each of these cases the values are conform to the S- and C-types of the corresponding families.

As an additional source of information, we used a large database of the Sloan Digital Sky Survey (SDSS) five broad-band photometry (e.g. Ivezić et al., 2001; Jurić et al., 2002) to characterize reflectance of smaller asteroids inside our families. We use the same methodology and data analysis as in Nesvorný et al. (2005), though we make advantage of the third, updated release of the SDSS data. This source contains five color information about 43424 individual moving objects that were positively identified with known sources. Searching in this database, we found information about the following numbers of asteroids in the studied families: Erigone – 104, Massalia – 301, Merxia – 83, and Astrid – 20. For each of them, we constructed normalized reflectance spectra and computed their principal components  $PC_1$  and  $PC_2$  (see Eq. (1) in Nesvorný et al., 2005a). For the final analysis we choose only objects with formal  $PC_1$  and  $PC_2$  errors smaller than 0.1. This translates into 36 objects in the Erigone family, 62 in the Massalia family, 32 in the Merxia family, and 6 in the Astrid family. In the Erigone family we found 6 data-points significantly shifted from the remaining ones toward large value of  $PC_1$  parameter, seemingly interloper S-type asteroids inside this family. Interestingly, this confirms guessed interlopers among the open circles in Fig. 4 for  $a < 2.36$  AU.

Figure 13 shows all these data together projected onto the plane of principal components  $PC_1$  and  $PC_2$ ; our four families go along with different colors. Assuming membership in a family represents a parametric relation between  $PC_1$  and  $PC_2$ ,

as an expression of common surface mineralogy, we identify the families as distinct cluster in this space of spectral parameters in the same way as the families are clusters in the space of proper orbital elements. From the available data, and upon elimination of few clear outliers, we can construct 90% confidence level zones for each of the families where any further measurements are expected (see e.g. Bertotti et al., 2003, Sec. 20.5). These are the color-coded ellipses in Fig. 13 that help us to better “delimit” family locations in the  $(PC_1, PC_2)$  space. The vertical dashed line at  $PC_1 = 3$  is also important since it marks a division between the S-complex (for which  $PC_1 > 3$ ) and C-complex (for which  $PC_1 < 3$ ; e.g. Binzel and Bus, 2002; Nesvorný et al., 2005). Except for a small overlap, perhaps due to few remaining interlopers, the 90% confidence levels of Erigone and Astrid families lie well within the C-complex zone and the Massalia and Merxia families reside in the S-complex zone. Indeed, the respective families were classified this way by Monthé-Diniz et al. (2005), who used a recent compilation of the most wealthy narrow-band spectroscopy databases SMASS and S3OS2.

The crosses in Fig. 13 show mean  $PC_1$  and  $PC_2$  in the respective family with their standard errors. This information is interesting in the context of our work, because Jedicke et al. (2004) and Nesvorný et al. (2005) related these mean values to the age of the family as an expression of the space weathering evolution. Borrowing their relation, we expect the Massalia and Merxia families to be of a similar age, different perhaps by only  $\sim 50\%$  or less, while the age of Erigone family might be an order of magnitude larger than that of the Astrid family. Obviously, the  $PC_1$ –age relation brought by Nesvorný et al. (2005) is empirical, and fluctuations about the mean trend could be expected. Also, these authors used a more approximate means to derive ages of the asteroids families, while it is a purpose of this paper to refine them for the four cases discussed.

#### 4. Selected families: Best-fit models

After having characterized our target families, we are now ready to apply the method outlined in Sec. 2.

#### 4.1. Erigone

Figure 14 shows the contour plots of  $\Psi_{\Delta C}$  projected onto 2-D parameter planes  $T$  vs.  $c_{\text{YORP}}$ ,  $T$  vs.  $V$  and  $c_{\text{YORP}}$  vs.  $V$ . The best-fit solution for  $N(C)$ , together with the observed data  $N_{\text{obs}}(C)$  and their formal error-bars, is shown in the same figure (left and top). At first we assume a constant geometric albedo  $p_V = 0.05$  and thermal conductivity  $K = 0.05$  W/m/K for all asteroids. In the contour plots we each time picked the best  $\Psi_{\Delta C}$ -value along the suppressed dimension. The “critical” isoline value of 21 is plotted in bold (recall this value formally corresponds to solutions that barely match the observed family at the chosen  $\sigma$ -interval from all data points). If we adopted this threshold correct, the best solution we obtain for the three parameters is:  $T = 340_{-40}^{+60}$  My,  $c_{\text{YORP}} = 0.8_{-0.5}^{+1.2}$  and  $V = 32_{-17}^{+8}$  m/s. Note, the three parameters are not uncorrelated in our solution, such that stronger YORP ( $c_{\text{YORP}}$ ) pushes the family age ( $T$ ) to smaller values. The least correlated are  $c_{\text{YORP}}$  and  $V$ . We also note that the strength of the YORP effect is weakly constrained, but its null value strongly disagrees with the observations (some minimum YORP effect is definitely needed to produce the displaced maximum in  $\Psi_{\Delta C}$ ). The best-fit velocity  $V$  is rather low, but compatible with expected values from the hydrocode modeling. The initial family thus had about half extension in semimajor axis than the currently observed one.

The best-fit value of the target function (12) we found is  $\Psi_{\Delta C} = 7.3$ , significantly smaller than 21, though we obviously admit a slight arbitrariness in our definition of formal standard deviation  $\sqrt{N_{\text{obs}}(C)}$  of number of objects in the  $C$ -strips (obviously any linear scaling in this quantity projects quadratically in the value of  $\Psi_{\Delta C}$ ). Nevertheless, we consider our fit statistically significant.

Next, we tested robustness of the solution as regards to changes in the surface thermal conductivity  $K$  (Fig. 15). We chose here a random value of  $K$  in between 0.005 and 0.05 W/m/K, making the average little lower than before. Our best solution now reads:  $T = 280_{-50}^{+30}$  My,  $c_{\text{YORP}} = 0.6_{-0.2}^{+1.4}$  and  $V = 26_{-11}^{+14}$  m/s. The minimum target function value is now  $\Psi_{\Delta C} = 6.8$ , again about a factor 3 lower than the statistically admissible value 21.

While the solutions for  $V$  and  $c_{\text{YORP}}$  parameters did not change much, the estimated age of the family  $T$  shifted to a smaller value. The same would happen should we assume a larger mean value of the geometric albedo  $p_V$  in the family. Our experiments show that  $T \propto p_V^{-a}$ , where  $a \sim 0.5$ . This approximate scaling law would have been expected if the Yarkovsky/YORP effects play significant role in determining the current family distribution since the strength of the Yarkovsky forces scale inversely proportionally with size of the bodies. The above relation is, however, approximate only and may also depend on the chosen family, reflecting different proportion in the total extent attributed to the initial velocity dispersion and Yarkovsky/YORP evolution. Since it is unlikely the mean albedo is much smaller than  $\sim 0.05$  used above, the 400 My represents an approximate upper limit for the age of this family. With  $p_V \sim 0.1$  and our lowest assumed thermal conductivity of 0.005 W/m/K, we obtain  $160_{-30}^{+30}$  My age for Erigone. Unfortunately, the burden of unknown geometric albedo, and to a lesser extent surface thermal conductivity, cannot be circumvent in our method and with currently available data. At the current state of things, we must conclude that the age of Erigone is  $\sim 280$  My with an uncertainty of  $\sim 40\%$ . Previous tests show that an intrinsic capability of our method would be – in the case of known mean  $p_V$  and  $K$  values – to determine the age at a  $\sim 10\%$  level.

## 4.2. Massalia

Figure 16 shows the distribution  $N_{\text{obs}}(C)$  of the Massalia members in the  $C$ -parameter from Eq. (2) ( $\beta = 1$ ) with errors bars amounting to  $\sqrt{N_{\text{obs}}(C)}$ . Unlike in the Erigone case, here we observe an asymmetry about  $C = 0$  so that at positive  $C$  values (thus  $a$  larger than  $a_c$ ) the bins are deficient in number of objects. Figures 2 and 6 tell us why this happens: the family is cut by a weak exterior M1/2 mean motion resonance with Mars that likely caused small but non-negligible leakage of asteroids from the family. The amount of objects drained from the family is generally unknown and its estimate is model-dependent. For that reason we decided to completely discard the  $C > 0$  data from our analysis and concentrate to fit only the  $C < 0$  distribution.

Figure 17 shows our solution that assumes all

asteroids having the same geometric albedo  $p_V = 0.21$  (as inferred for Massalia) and surface thermal conductivity  $K = 0.005$  W/m/K. The best-fit solution minimizes the target (12) to  $\Psi_{\Delta C} = 9.3$ , to be compared to the critical value of 24 (i.e. number of data points). The solved-for parameters have then the following values:  $T = 152_{-18}^{+18}$  My,  $c_{\text{YORP}} = 0.2_{-0.1}^{+1.8}$  and  $V = 17_{-5}^{+5}$  m/s. Except for  $c_{\text{YORP}} \sim 0$ , which is surely excluded, the match of Massalia’s data does only weakly constrain the strength of the YORP effect. On the other hand, the family age  $T$  and the velocity parameter  $V$  are surprisingly well constrained. This solution nearly does not change if the surface thermal conductivity  $K$  is allowed to randomly span an interval 0.001 – 0.01 W/m/K. Should Massalia have an anomalously large geometric albedo in the family, so that, for instance, the mean geometric albedo of smaller members in the family was  $p_V \sim 0.12$ , we would obtain the following best-fit parameter values:  $T = 190_{-20}^{+40}$  My,  $c_{\text{YORP}} = 0.5_{-0.3}^{+1.5}$  and  $V = 25_{-8}^{+5}$  m/s. We thus conclude that the upper limit for the Massalia age is  $\sim 240$  My, but we find more likely the true age is  $\sim 150 - 200$  My.

Massalia’s size is 145.5 km (Tedesco et al. 2002). Durda et al. (2005, in preparation) estimate it represents nearly 99% of the family parent object mass (slightly more than Tanga et al. (1999) who give 90%), so that the family is a result of a big cratering event. This may result in a somewhat lower fitted value of the velocity dispersion parameter  $V$  as compared to the Erigone family, whose parent body had likely only  $\sim 110$  km in size.

Analysis of the Massalia age is of particular interest because this family has been proposed as an alternative source for the  $\alpha$  dust band (e.g. Nesvorný et al., 2003), competing the Themis family. Given the estimate of ratio of the parent-bodies respective sizes, and a very old age of the Themis family, the age of Massalia family becomes critical in judging if the dust production in this zone can be higher than in the Themis family. However, we postpone considerations whether the Massalia’s cratering event could have produced enough dust to feed the  $\alpha$  dust band to a future work.

### 4.3. Merxia

Similarly to Erigone, Merxia family exhibits the  $N_{\text{obs}}$  distribution symmetric enough that we fold negative and positive  $C$  values into a single bin without a loss of information (Fig. 18; upper and left panel). The other panels of the same figure than show our solution that assumes all asteroids having the same geometric albedo  $p_V = 0.22$  (as inferred for 808 Merxia) and surface thermal conductivity  $K = 0.005$  W/m/K. The best-fit solution minimizes the target function (12) to  $\Psi_{\Delta C} = 3.9$ , to be compared to the critical value of 17 (number of data points). The solved-for parameters have then the following values:  $T = 238_{-23}^{+52}$  My,  $c_{\text{YORP}} = 0.6_{-0.4}^{+1.4}$  and  $V = 24_{-12}^{+6}$  m/s. The overall character of the solution is similar to those described above. For instance the Merxia solution is robust against a change in the thermal conductivity: should we assume a random value in between 0.001–0.01 W/m/K interval, rather than the fixed, midpoint value as above, we would get a solution shown in Fig. 19. The best-fit values and their uncertainty intervals changed only insignificantly. In a less likely case when all smaller members of the Merxia family would have systematically smaller surface albedo, such as  $p_V \sim 0.12$  for instance, the best fits age of the family would become  $T = 325_{-50}^{+75}$  My with other parameters about the same as before. Our solution thus does not support an age longer than  $\sim 400$  My for the Merxia family.

In general, our respective solution for the Massalia and Merxia family ages confirm previously guessed  $\sim 50\%$  difference toward a younger Massalia (Sec. 3).

### 4.4. Astrid

Figure 20 shows the  $N_{\text{obs}}(C)$  distribution for the Astrid family. Here we again encounter an asymmetry about  $C = 0$  value, but now even more pronounced than in the Massalia case (Fig. 16). The reason is a significant underpopulation of the high semimajor axis end of this family (Fig. 11). In Sec. 5.4 we search for a putative dynamical mechanism to deplete the zone between the Astrid family and the J5/2 mean motion resonance but we fail to find any. There is certainly a possibility of initially anisotropic velocity field in this family, but it remains unclear while the left side of the

family ( $a \leq 2.787$  AU) is so much more populated if now depletion mechanism is at place. We tentatively use this left part of the family in our analysis (thus  $\mathcal{D}(C)$  with  $C < 0$ ), but we are aware that these results are least certain in our paper.

Figure 21 shows our solution for  $p_V = 0.08$  and  $K = 0.05$  W/m/K uniformly assigned to all Astrid members. The best-fit solution minimizes the target (12) to  $\Psi_{\Delta C} = 1.3$ , to be compared to the critical value of 11 (number of data points). The solved-for parameters have the following values:  $T = 214_{-44}^{+116}$  My,  $c_{\text{YORP}} = 0.9_{-0.9}^{+1.1}$  and  $V = 13_{-13}^{+12}$  m/s. Here the solution is the poorest from all our cases, possibly because number of constraining asteroids became small after having been forced to eliminate  $C > 0$  bodies. The characteristic velocity  $V$  of the  $D \sim 5$  km fragment initial ejection is smaller than in the Merxia and Erigone cases. This may be due to the fact that the parent body of the Astrid family was only  $\sim (60-70)$  km in size (Durda et al., 2005, in preparation). Assuming the surface thermal conductivity of Astrid asteroids randomly ranges 0.005–0.05 W/m/K, the age becomes  $T = 180_{-40}^{+80}$  My, with further decrease if mean geometric albedo is higher than 0.08. This possibility, however, does not seem likely for a C-type family.

If the initial velocity field was anisotropic, tilting the initial member distribution distorted toward  $a < a_c = 2.787$  AU, our result would overestimate the family age. A factor 2 is not excluded, so that the Astrid family may be as young as  $\sim 100$  My (e.g. Nesvorný et al., 2005).

## 5. Selected families: Additional simulations

In this section we complement, and strengthen in some cases, our model of Yarkovsky dispersion of the chosen families by direct numerical integration of orbits for a limited number of family asteroids. In particular, these results explain some peculiar features noted earlier.

We use a SWIFT-RMVS integrator (e.g. Levison and Duncan, 1994) modified to account for the Yarkovsky forces and with a second order symplectic map due to Laskar and Robutel (2001; see <http://sirrah.troja.mff.cuni.cz/yarko-site/> for details of the implementation, rapidity and accuracy tests). We also comple-

mented the original version of the integrator with an on-line computation of synthetic proper elements in a way compatible with a definition of Knežević and Milani (2000, 2003). This means we first apply a Fourier filter to the (non-singular) orbital elements in a moving window of  $\simeq 0.7$  My (with steps of 0.1 My) to eliminate all periods smaller than some threshold (1.5 ky in our case). The filtered signal is output from the simulation for further checks and passed through a frequency analysis code adapted from Šidlichovský and Nesvorný (1997) to obtain (planetary) forced and free terms in Fourier representation of the orbital elements. The isolated free terms are what we use as the proper orbital elements.

In the case of Erigone and Massalia, families in the inner part of the main belt, all planets except for Mercury and Pluto are included in our simulation with their masses, initial positions and velocities taken from the JPL DE405 ephemerides. A timestep of 0.05 yr is used. In the case of Merxia and Astrid, families in the central part of the main belt, we included outer planets in our simulation only and used longer integration timestep of 0.25 yr. To set initial orbital conditions for test bodies we select a limited number of real asteroids, members of the corresponding family. We also use a number of fictitious objects whose orbital elements were created by tiny changes in semimajor axis and eccentricity of real objects; in line of a common terminology we call them “clones”. Typically, 100 – 200 test bodies are integrated for a couple of hundred My. When Yarkovsky forces are included in the simulation we use a range of characteristic sizes of members in the family that interest us – typically 2–20 km. Rotation rates are assumed Maxwellian with a peak value corresponding to a period of 8 hr (though we prevent shorter/longer periods than 4/12 hr). In the Massalia, Merxia and Astrid cases we purposely want bodies migrate toward larger values of the semimajor axis. To make the semimajor axis drift “typical” we set obliquities  $\simeq 45^\circ$ ; this underestimates the maximum possible drift rate by the diurnal variant of the Yarkovsky effect by a factor of  $\simeq \sqrt{2}$ . Thermal parameters, necessary for modeling Yarkovsky forces, are: thermal conductivity  $K = 0.005$  W/m/K, specific heat capacity  $C_p = 680$  J/kg/K, surface and bulk densities 1.5 and 2.5 g/cm<sup>3</sup>. This is about

the best guess we can do for multikilometre asteroids in the main asteroid belt, but we argue small changes in these value do not modify our conclusions. We use analytic formulae of Vokrouhlický (1998, 1999) and Vokrouhlický and Farinella (1999; Appendix) for both diurnal and seasonal variants of the Yarkovsky effect.

### 5.1. Erigone

The purpose of Erigone simulation was to remove suspicion that the remarkable depletion in the center of the family (Fig. 4), interpreted by our model as the synergy of the Yarkovsky/YORP effects, might be alternatively explained using depletion through weak mean motion resonances. The work of Morbidelli and Nesvorný (1998) suggests there are no such resonances near the center of this family, but our direct simulation checks in detail this conclusion.

Unlike below, we thus do not include thermal forces in our simulation and we numerically integrate conservative system where only gravitational interactions are taken into account. We select 108 asteroids, and their close clones, in the void central zone of the family and propagate their orbits for 500 My in the future. Figure 23 shows the resulting evolutionary tracks projected onto planes of proper semimajor axis  $a$  vs proper eccentricity  $e$  and proper semimajor axis  $a$  vs proper sine of inclination  $\sin I$ . In some cases these tracks stay very near the initial point indicating a very high degree of stability in this particular region. At the high-eccentricity end of the family the synthetic proper elements indicate larger, but stable oscillations. These are triggered by interaction with the high-order secular resonance  $z_2 = 2(g-g_6) + s - s_6$  (e.g. Milani and Knežević, 1994). In fact, we hypothesize, that the systematically lower upper bound in proper eccentricity for  $a \leq a_c \simeq 2.37$  AU is just caused by the  $z_2$  resonance that efficiently captures Yarkovsky-moving asteroids (see the similar role of the  $z_1$  resonance in the Eos family; Vokrouhlický et al., 2005). Our integration, however, suggests that without thermal effects this resonant effect is very stable on a long-term. As a result, none of the objects evolved enough to escape from the family. Although our integrated timespan is still shorter than the age of the Solar system, we dare to extrapolate our result and claim there is basically no depletion in the cen-

tral region of the Erigone family. In fact, this is a very fortuitous circumstance, because it allows us to convincingly show that other mechanism must have created the bipolar distribution of small asteroids in this family.

## 5.2. Massalia

In Sec. 3.2 we noted that the Massalia family has been clearly affected by the exterior mean motions resonance M1/2 with Mars located at  $a \simeq 2.42$  AU. A stream of asteroids is seen “radiating” from the family along this resonance along inclination values (Fig. 6). In Sec. 4.2 we determined that the  $\mathcal{D}(C)$  distribution is markedly asymmetric about  $C = 0$  with lower peak value for positive  $C$  (thus  $a > a_c \simeq 2.407$  AU). We associated this asymmetry with the previously noted leakage through the M1/2 resonance and for that reason decided to use only the  $C < 0$  values of  $\mathcal{D}(C)$  distribution, unaffected by this process. In this section we aim to verify that the observed structure in the Massalia family is compatible with these ideas within our model of Yarkovsky-driven expansion of an initially compact family.

We selected 137 Massalia members in its central zone. Orbits of these particles have been numerically propagated for 240 My, an approximate age of this family (Sec. 4.2). The bodies had sizes ranging an interval of 0.7 – 9 km, and rotational and thermal parameters as stated above.

Figure 24 shows result of our experiment. The orbital tracks shown in this figure use double coding: (i) black – when, at that stage, the body is still associated with the real Merxia family at the HCM cutoff velocity  $V_c = 44$  m/s (corresponding to our nominal family) and (ii) gray – when orbital parameters changed enough so that the minimum HCM distance to any of the family members exceeds  $V_c = 44$  m/s. The later would show a fate of bodies escaping from the nominal family. We confirm that upon reaching the M1/2 resonance, some orbits get dispersed so that they cease to be identified as family members. This has happened in 22 out of 136 cases which represents some 16% of all integrated orbits. This may partly explain the asymmetry of the  $N_{\text{obs}}(C)$  distribution from Fig. 16. As time will proceed, part of the family members will fall in the J3/1 mean motion resonance at  $a \simeq 2.48$  AU. The current family is right on the brink of that situation.

## 5.3. Merxia

In this case, our goal is to make understand the higher dispersion of the family members’ proper eccentricity  $e$  and, to a lesser extend, proper inclination  $I$  values beyond the three-body resonance 3J-1S-1 ( $a \simeq 2.75$  AU; Figs. 2 and 8). Our working hypothesis is that majority of members initially landed below this resonance (i.e. had  $a < 2.75$  AU) and some migrated toward larger  $a$ -values by the Yarkovsky forces. Upon reaching this resonance, they might have temporarily interacted with it, sliding toward smaller and larger eccentricity and inclination values. When leaving the 3J–1S–1 resonance, their  $e$ - and  $I$ -distributions would freeze information about this resonant interaction.

Figure 25 shows evolution of 145 orbits over 250 My, a timespan compatible with our best estimate for this family age. Initial data are several real asteroids associated with the family, residing near its center, each of which has been cloned by small changes in orbital semimajor axis and eccentricity. Our test bodies had sizes in the range 1.5–20 km and rotational and thermal parameters as stated above. We again use the black/gray coding for segments of the evolutionary track that are (or are not) associated with the nominal family.

Our results indicate that 34 out of 127 drifting orbits that encountered the 3J–1S–1 resonance were eliminated from the family (i.e. some 27%). An important result is that the eccentricity and inclination dispersion becomes significantly larger and well compatible with the observed family members beyond the 3J–1S–1 resonance. This merely confirms our hypothesis and strongly supports our model based on Yarkovsky/YORP dispersion of the families. Interestingly though, the  $N_{\text{obs}}(C)$  distribution of the Merxia family is nearly symmetric about  $C = 0$  (with only  $\sim 5\%$  less bodies for  $C > 0$ ), as if the rate of asteroid elimination from the family by the 3J–1S–1 resonance should have been smaller than found in our simulation. We find likely, that some asteroids were initially thrown beyond this resonance and did not underwent interaction with it.

## 5.4. Astrid

The main puzzle of the Astrid family stems from its asymmetry in  $\mathcal{D}(C)$  about  $C = 0$ , or in

other words asymmetry in the semimajor axis distribution about  $a_c \simeq 2.787$  AU (position of 1128 Astrid; Fig. 11). There are no major, in fact even minor, mean motion resonances crossing this family to trigger depletion for  $a \geq a_c$ . The powerful J5/2 mean motion resonance with Jupiter is close-by, but still its separatrix at  $\sim 2.82$  AU is more than  $\sim 0.015$  AU distant from the closest Astrid members. The family thus does not adhere to this resonance. Even more puzzling is that fact that the zone in between the Astrid family and the J5/2 resonance is entirely void of any (family or background) objects.

We first suspected there is a more complex resonance –such as the high-order secular resonance– just above the Astrid family that quickly transports objects into the J5/2 mean motion resonance and thus provides significant depletion<sup>5</sup>. Our direct numerical simulation of 110 asteroids, Astrid members, and their clones however does not support this idea. In Fig. 26 we show evolutionary tracks of these particles integrated over 200 My timespan. Their sizes range 3 – 12 km and obliquities were set to  $\sim 45^\circ$  to purposely make them migrating toward the J5/2 resonance. Except for effect of a few very weak resonances, we do not detect any noticeable perturbation prior a fall into J5/2. From the dynamical standpoint, the Astrid family is well allowed to extend toward the J5/2 resonance and the same applies to any background body. With no dynamical process that would prohibit populating the zone above the Astrid family, the void region there appears anomalous and needs explanation. In the same time, the odd structure of the Astrid family seems to require an internal reason.

We also note that migration toward higher semimajor axis value requires prograde spin state. Using the same integrator as in Vokrouhlický et al. (2003) we checked there is no global instability in the prograde-rotation states for Astrid members. In fact, the phase space of rotation states looks very similar to that in the Koronis family (just above the J5/2 resonance) where prograde rotation states exist and are trapped in the spin-orbit

<sup>5</sup>Recall e.g. the case of  $g + 2g_5 - 3g_6$  secular resonance in the Koronis family that is able to quasi-instantly lift proper eccentricity by a significant value, thereby –if located on the upper side of the Astrid family– send asteroids right to the J5/2 resonance.

secular resonance  $s_6$ . A similar situation might have happened for Astrid, making obliquities for most of the upward migrating asteroids near  $\sim 50^\circ$  and thus not allowing them to migrate at maximum rate. This could have contributed to the asymmetry seen in the family as far as extension in  $a$  from  $a_c$  is concerned. On the other hand, migration toward higher semimajor axis values seems not being prohibited and more than a factor 2 of objects with  $a \leq a_c$  and compared to those with  $a \geq a_c$  is still anomalous. It requires either highly anisotropic initial velocity field and/or asymmetry in the initial spin axis distribution. Both are possible, but their detailed study goes beyond this paper. An peculiarly high thermal conductivity of Astrid members might be also an unusual explanation of the data, because the seasonal variant of the Yarkovsky effect drives bodies toward the Sun only (see already Farinella and Vokrouhlický, 1999).

## 6. Discussion

In this paper, we studied structure of four young families and demonstrated capability of the combined Yarkovsky and YORP evolution model to valuably constrain some important parameters. As regards the age of the family, our method may potentially yield  $\sim 10\%$  accurate results if there were not uncertainties in the surface parameters of the member asteroids (albedo and thermal conductivity). Nevertheless, our age estimates in the four cases analysed above are still the best available values.

We find it interesting, that our search dated two asteroid families – Erigone and Merxia – with parent bodies larger than 100 km younger than 1 Gy. Moreover, we have Veritas family a borderline case between cratering event and catastrophic disruption with the age of 8.3 My (Nesvorný et al., 2003), and Massalia, a big cratering event, within the last 1 Gy. We believe our search for such events is nearly complete, and we might have missed one or two more cases because of mean motion resonances cutting the families and preventing application of our method. This number compares very well with a recent work of Bottke et al. (2005a,b), who found, by considering collisional evolution of the main asteroid belt in the past 4.5 Gy, that about 3 – 4 asteroid families with parent bodies

larger than 100 km should have been created in the past 1 Gy.

Unavoidably a question pops out why we have not applied our method systematically to all known asteroid families? Generally, it is not possible. Obviously, this does not mean our method is mistaken, it only means that it relies on certain conditions that are not satisfied in all possible age regimes.

First, we point out there might be few more cases where our method is applicable. Agnia and Naema families indicate a similar structure as the four families studied in this work, however, their analysis would require some caution that goes beyond the extend of this text. For instance, the Agnia family is fully embedded inside the high-order secular resonance  $z_1$  (e.g. Milani and Knežević, 1994) and that might have affected its evolution to an extent that needs to be studied. Also, parent bodies of these families were smaller, a few tens of kilometres in size, so that –like in the Astrid case– the majority of members are small asteroids. Further discoveries and proper element computations will help to define these families better than today.

Second, there are two regimes of age to which our method is not adapted. Very young families, with ages less than  $\simeq 50$  My such as Karin, Veritas or Iannini, did not evolve enough by the thermal forces to produce the required offset in extremes of the  $N_{\text{obs}}(C)$  distribution that is fitted in our approach. Obviously, the thermal forces do perturb all asteroid orbits, including those in the very young families, but the means to detect them are different than used here (see Nesvorný and Bottke, 2004). On the contrary, old families, with ages greater than  $\simeq 1$  Gy, did evolve “too much” by the thermal forces. A good example is the Themis family, whose age is estimated to be  $\sim (2.5 \pm 1.0)$  Gy (e.g. Nesvorný et al., 2005) and whose projection onto the proper semimajor axis  $a$  vs. absolute magnitude  $H$  is shown in Fig. 27. The family shows a typical bracketing by powerful mean motion resonances (J2/1, J11/5 and 3J–2S–1). One can also see the distinct feature of a relative under-population in the middle- $a$  values and a relative overpopulation in the extreme- $a$  values for asteroids with  $H \geq 12.5$ .

To see the obstacle, we recall these features result from a synergy between Yarkovsky effect secular changes in semimajor axis enhanced by the

YORP effect tilting spin axes toward the extreme-obliquity values. As those asymptotic values are reached, YORP continues to either accelerate or decelerate asteroid’s rotation to the point when the rotation state should dramatically change by either collisional impact, structural alterations or even fission. In either of these cases, our ability to model the result is poor so far. Vokrouhlický and Čapek (2002), and Čapek and Vokrouhlický (2004), have estimated that a typical timescale of such “YORP cycle” for  $\sim 5$  km objects is  $\sim (300–600)$  My. So in the case of families studied in Sec. 4 their age is about the length of the YORP cycle for asteroids defining the  $N_{\text{obs}}(C)$  distribution. Our inability to accurately model the result of YORP-cycle termination and onset of a new YORP-cycle is not critical. Here however, for a  $\sim 2.5$  Gy old family, such as Themis, one could expect small members has undergone 5 to 8 YORP cycles during its lifetime. Here, our inability to accurately model a sequence of YORP cycles becomes important and it could result in misleading conclusions. For instance, if we formally attempt to use our method in the Themis case we would obtain a poor fit (so that the minimum found value of the target function  $\Psi_{\Delta C}$  would be larger than number of data points) and  $c_{\text{YORP}} \sim 0$  expressing inadequacy in the YORP modelling.

Another result in this paper is a confirmation of small initial dispersal velocities in the studied families. A typical velocity  $V$  of  $\sim 5$  km fragments was found a few tens of m/s. This value is compatible with hydrocode modelling and means the initial semimajor axis dispersal in our families was about 25 – 50% of the currently observed value.

This work has been supported by the Grant Agency of the Czech Republic (grant 205/05/2737) and ...

## REFERENCES

- Bahcall, J.N., Pinsonneault, M.H., Basu, S., 2001. Solar models: Current epoch and time dependences, neutrinos, and helioseismological properties. *Astrophys. J.* 555, 990–1012.
- Bendjoya, P., Zappalà, V., 2002. Asteroid family identification. in: *Asteroids III* (W.F. Bottke, A. Cellino, P. Paolicchi and R.P. Binzel, Eds.), pp. 613–618. Arizona University Press, Tucson.

- Benz, W., Asphaug, E., 1999. Catastrophic disruptions revisited. *Icarus* 142, 5–20.
- Bertotti, B., Farinella, P., Vokrouhlický, D., 2003. *Physics of the Solar System*. Kluwer Academic Publishers, Dordrecht.
- Binzel, R.P., 1987. The Koronis family: Possible evidence for a recent catastrophic disruption. *Lunar and Planetary Institute Conference Abstracts* 18, 77.
- Binzel, R.P., 1988. Collisional evolution in the Eos and Koronis asteroid families – Observational and numerical results. *Icarus* 73, 303–313.
- Bottke, W.F., Vokrouhlický, D., Brož, M., Nesvorný, D., Morbidelli, A., 2001. Dynamical spreading of asteroid families via the Yarkovsky effect: The Koronis family and beyond. *Science* 294, 1693–1695.
- Bottke, W.F., Vokrouhlický, D., Rubincam, D.P., Brož, M., 2002. Dynamical evolution of asteroids and meteoroids using the Yarkovsky effect. in: *Asteroids III* (W.F. Bottke, A. Cellino, P. Paolicchi and R.P. Binzel, Eds.), pp. 395–408. Arizona University Press, Tucson.
- Bottke, W.F., Durda, D.D., Nesvorný, D., Jedicke, R., Morbidelli, A., Vokrouhlický, D., Levison, H.F., 2005a. The fossilized size distribution of the main asteroid belt. *Icarus*, in press.
- Bottke, W.F., Durda, D.D., Nesvorný, D., Jedicke, R., Morbidelli, A., Vokrouhlický, D., Levison, H.F., 2005b. The collisional evolution and dynamical depletion of the main belt: Constraints on the initial population and formation time of Jupiter. *Icarus*, submitted.
- Brouwer, D., 1951. Secular variations of the orbital elements of minor planets. *Astron. J.* 56, 9–32.
- Bus, S.J., Binzel, R.P., 2002. Phase II of the small main-belt asteroid spectroscopic survey. The observations. *Icarus* 158, 106–145.
- Čapek, D., Vokrouhlický, D., 2004. The YORP effect with finite thermal conductivity. *Icarus*, in press.
- Carruba, V., Burns, J.A., Bottke, W.F., Nesvorný, D., 2003. Orbital evolution of the Gefion and Adeona asteroid families: close encounters with massive asteroids and the Yarkovsky effect. *Icarus* 162, 308–327.
- Cellino, A., Bus, S.J., Doressoundiram, A., Lazzaro, D., 2002. Spectroscopic properties of asteroid families. in: *Asteroids III* (W.F. Bottke, A. Cellino, P. Paolicchi and R.P. Binzel, Eds.), pp. 633–643. Arizona University Press, Tucson.
- Cellino, A., Michel, P., Tanga, P., Zappalà, V., Paolicchi, P., Dell’Oro, A., 1999. The velocity-size relationship for members of asteroid families and implications for the physics of catastrophic collisions. *Icarus* 141, 79–95.
- Chapman, C.R., 2003. Cratering on asteroids from Galileo and NEAR Shoemaker. in: *Asteroids III* (W.F. Bottke, A. Cellino, P. Paolicchi and R.P. Binzel, Eds.), pp. 315–330. Arizona University Press, Tucson.
- Chapman, C.R., 2004. Space weathering of asteroid surfaces. *Annu. Rev. Earth Planet. Sci.* 32, 539–567.
- Chapman, C.R., Ryan, E.V., Merline, W.J., Neukum, G., Wagner, R., Thomas, P.C., Veverka, J., Sullivan, R.J., 1996. Cratering on Ida. *Icarus* 120, 77–86.
- Chapman, C.R., Veverka, J., Belton, M.J.S., Neukum, G., Morrison, D., 1996. Cratering on Gaspra. *Icarus* 120, 231–245.
- Davis, D.R., Farinella, P., Paolicchi, P., Weidenschilling, S.J., Binzel, R.P., 1989. Asteroid collisional history: Effects on sizes and spins. in: *Asteroids II* (R.P. Binzel, T. Gehrels and M.S. Matthews, Eds.), pp. 805–826. Arizona University Press, Tucson.
- Dell’Oro, A., Bigongiari, G., Paolicchi, P., Cellino, A., 2004. Asteroid families: evidence of ageing of the proper elements. *Icarus* 169, 341–356.
- Dohnanyi, J.W., 1969. Collisional models of asteroids and their debris. *J. Geophys. Res.* 74, 2531–2554.
- Farinella, P., Vokrouhlický, D., 1999. Semimajor axis mobility of asteroidal fragments. *Science* 283, 1507–1510.

- Farinella, P., Vokrouhlický, D., Hartmann, W.K., 1998. Meteorite delivery via Yarkovsky orbital drift. *Icarus* 132, 378–387.
- Farinella, P., Carpino, M., Froeschlé, Ch., Froeschlé, C., Gonczi, R., Knežević, Z., Zappalà, V., 1989. The ages of asteroid families. *Astron. Astrophys.* 217, 298–306.
- Haack, H., Farinella, P., Scott, E.R.D., Keil, K., 1996. Meteoritic, asteroidal, and theoretical constraints on the 500 Ma disruption of the L chondrite parent body. *Icarus* 119, 182–191.
- Ivezić, Z., and 32 collaborators. Solar system objects observed in the Sloan Digital Sky Survey commissioning data. *Astron. J.* 122, 2749–2784.
- Jedicke, R., Nesvorný, D., Whiteley, R., Ivezić, Z., Jurić, M., 2004. An age-colour relationship for main-belt S-complex asteroids. *Nature* 429, 275–277.
- Jurić, M., and 12 collaborators, 2002. Comparison of positions and magnitudes of asteroids observed in the Sloan Digital Sky Survey with those predicted for known asteroids. *Astron. J.* 124, 1776–1787.
- Knežević, Z., Milani, A., 2000. Synthetic proper elements for outer main belt asteroids. *Celest. Mech. Dyn. Astron.* 78, 17–46.
- Knežević, Z., Milani, A., 2003. Proper element catalogs and asteroid families. *Astron. Astrophys.* 403, 1165–1173.
- Knežević, Z., Lemaître, A., Milani, A., 2002. The determination of asteroid proper elements. in: *Asteroids III* (W.F. Bottke, A. Cellino, P. Paolicchi and R.P. Binzel, Eds.), pp. 603–612. Arizona University Press, Tucson.
- Laskar, J., Robutel, P., 2001. High order symplectic integrators for perturbed Hamiltonian systems. *Celest. Mech. Dyn. Astr.* 80, 39–62.
- Levison, H., Duncan, M., 1994. The long-term dynamical behavior of short-period comets. *Icarus* 108, 18–36.
- Love, S.G., Ahrens, T.J., 1996. Catastrophic impacts on gravity dominated asteroids. *Icarus* 124, 141–155.
- Marzari, F., Davis, D.R., Vanzani, V., 1995. Collisional evolution of asteroid families. *Icarus* 113, 168–187.
- Marzari, F., Cellino, A., Davis, D.R., Farinella, P., Zappalà, V., Vanzani, V., 1996. Origin and evolution of the Vesta asteroid family. *Astron. Astrophys.* 316, 248–262.
- Marzari, F., Farinella, P., Davis, D.R., 1999. Origin, aging, and death of asteroid families. *Icarus* 142, 63–77.
- Migliorini, F., Zappalà, V., Vio, R., Cellino, A., 1995. Interlopers within asteroid families. *Icarus* 118, 271–291.
- Milani, A., Knežević, Z., 1990. Secular perturbation theory and computation of asteroid proper elements. *Celest. Mech. Dyn. Astr.* 49, 347–411.
- Milani, A., Knežević, Z., 1992. Asteroid proper elements and secular resonances. *Icarus* 98, 211–232.
- Milani, A., Nobili, A.-M., 1992. An example of stable chaos in the Solar System. *Nature* 357, 569–570.
- Milani, A., Farinella, P., 1994. The age of Veritas asteroid family deduced by chaotic chronology. *Nature* 370, 40–42.
- Milani, A., Knežević, Z., 1994. Asteroid proper elements and the dynamical structure of the asteroid main belt. *Icarus* 107, 219–254.
- Milani, A., Nobili, A.-M., Knežević, Z., 1997. Stable chaos in the asteroid belt. *Icarus* 125, 13–31.
- Monthé-Diniz, T., Roig, F., Carvano, J.M., 2005. Reanalysis of asteroid families structure through visible spectroscopy. *Icarus*, in press.
- Morbidelli, A., 2002. *Modern Celestial Mechanics: Aspects of Solar System Dynamics*. Taylor & Francis, London.
- Morbidelli, A., Nesvorný, D., 1998. Three-body mean motion resonances and the chaotic structure of the asteroid belt. *Astron. J.* 116, 3029–3037.
- Morbidelli, A., Vokrouhlický, D., 2003. The Yarkovsky-driven origin of Near Earth Asteroids. *Icarus* 163, 120–134.

- Morbidelli, A., Zappalà, V., Moons, M., Cellino, A., Gonczi, R., 1995. Asteroid families close to mean motion resonances: Dynamical effects and physical implications. *Icarus* 118, 132–154.
- Morbidelli, A., Nesvorný, D., Bottke, W.F., Michel, P., Vokrouhlický, D., Tanga, P., 2003. The shallow magnitude distribution of asteroid families. *Icarus* 162, 328–336.
- Nesvorný, D., Morbidelli, A., 1999. Numerous weak resonances drive asteroids toward terrestrial planets orbits. *Icarus* 139, 295–308.
- Nesvorný, D., Bottke, W.F., 2004. Detection of the Yarkovsky effect for main-belt asteroids. *Icarus* 170, 324–342.
- Nesvorný, D., Morbidelli, A., Vokrouhlický, D., Bottke, W.F., Brož, M., 2002a, The Flora family: a case of the dynamically dispersed collisional swarm?, *Icarus* 157, 155–172.
- Nesvorný, D., Bottke, W.F., Dones, L., Levison, H.F., 2002b. The recent breakup of an asteroid in the main-belt region. *Nature* 417, 720–722.
- Nesvorný, D., Bottke, W.F., Levison, H.F., Dones, L., 2003. Recent origin of the Solar System dust bands. *Astrophys. J.* 591, 486–497.
- Nesvorný, D., Jedicke, R., Whiteley, R.J., Ivezić, Ž., 2005. Evidence for asteroid space weathering from the Sloan Digital Sky Survey. *Icarus* 173, 132–152.
- O’Brien, D.P., Greenberg, R., 2003. Steady-state size distributions for collisional populations: analytical solution with size-dependent strength. *Icarus* 164, 334–345.
- Petit, J.-M., Farinella, P., 1993. Modelling the outcomes of high-velocity impacts between small solar system bodies. *Celest. Mech. Dyn. Astr.* 57, 1–28.
- Pisani, E., Dell’Oro, A., Paolicchi, P., 1999. Puzzling asteroid families. *Icarus* 142, 78–88.
- Rubincam, D.P., 2000. Radiative spin-up and spin-down of small asteroids. *Icarus* 148, 2–11.
- Ryan, E.V., Melosh, H.J., 1998, Impact fragmentation: From the laboratory to asteroids. *Icarus* 133, 1–24.
- Slivan, S.M., 2002. Spin vector alignment of Koronis family asteroids. *Nature* 419, 49–51.
- Slivan, S.M., Binzel, R.P., 1996. Forty-eight new rotation lightcurves of 12 Koronis family asteroids. *Icarus* 124, 452–470.
- Slivan, S.M., Binzel, R.P., Crespo da Silva, L.D., Kaasalainen, M., Lyndaker, M.M., Krčo, M., 2003. Spin vectors in the Koronis family: comprehensive results from two independent analyses of 213 rotation lightcurves. *Icarus* 162, 285–307.
- Šidlichovský, M., Nesvorný, D., 1997. Frequency modified Fourier transform and its applications to asteroids. *Celest. Mech. Dyn. Astron.* 65, 137–148.
- Tanga, P., Cellino, A., Michel, P., Zappalà, V., Paolicchi, P., Dell’Oro, A., 1999. On the size distribution of asteroid families: The role of geometry. *Icarus* 141, 65–78.
- Tedesco, E.F., Noah, P.V., Noah, M., Price S.D., 2002. The supplemental IRAS minor planet survey. *Astron. J.* 123, 1056–1085.
- Vokrouhlický, D., 1998. Diurnal Yarkovsky effect as a source of mobility of meter-sized asteroidal fragments. I. Linear theory. *Astron. Astrophys.* 335, 1093–1100.
- Vokrouhlický, D., 1999. A complete linear model for the Yarkovsky thermal force on spherical asteroid fragments. *Astron. Astrophys.* 344, 362–366.
- Vokrouhlický, D., Farinella, P., 1998. The Yarkovsky seasonal effect on asteroidal fragments: A nonlinearized theory for the plane-parallel case. *Astron. J.* 116, 2032–2041.
- Vokrouhlický, D., Farinella, P., 1999. The Yarkovsky seasonal effect on asteroidal fragments: A nonlinearized theory for spherical bodies. *Astron. J.* 118, 3049–3060.
- Vokrouhlický, D., Čapek, D., 2002. YORP-induced long-term evolution of the spin state of small asteroids and meteoroids. Rubincam’s approximation. *Icarus* 159, 449–467.

- Vokrouhlický, D., Brož, M., 2002. Interaction of the Yarkovsky-drifting orbits with weak resonances: Numerical evidence and challenges. in: *Modern Celestial Mechanics: from Theory to Applications* (A. Celletti, S. Ferraz-Mello and J. Henrard, Eds.) pp. 467–472. Kluwer Academic Publishers, Dordrecht.
- Vokrouhlický, D., Nesvorný, D., Bottke, W.F., 2003. Thermal torques produce spin vector alignments among Koronis family asteroids. *Nature* 425, 147–151, 2003.
- Vokrouhlický, D., Brož, M., Morbidelli, A., Bottke, W.F., Nesvorný, D., Lazzaro, D., Rivkin, A.S., 2002. Yarkovsky footprints in the Eos family, Abstract No. 12.01 presented at the *Asteroids, Comets and Meteors* meeting, Berlin.
- Vokrouhlický, D., Brož, M., Morbidelli, A., Bottke, W.F., Nesvorný, D., Lazzaro, D., Rivkin, A.S., 2005. Yarkovsky footprints in the Eos family. *Icarus*, submitted.
- Zappalà, V., Cellino, A., Farinella, P., Knežević, Z., 1990. Asteroid families. I - Identification by hierarchical clustering and reliability assessment. *Astron. J.* 100, 2030–2046.
- Zappalà, V., Bendjoya, P., Cellino, A., Farinella, P., Froeschlé, C., 1995. Asteroid families: Search of a 12,487-asteroid sample using two different clustering techniques. *Icarus* 116, 291–314.
- Zappalà, V., Cellino, A., Dell’Oro, A., Migliorini, F., Paolicchi, P., 1996. Reconstructing the original velocity fields of asteroid families. *Icarus* 124, 156–180.
- Zappalà, V., Cellino, A., Dell’Oro, A., Paolicchi, P., 2002. Physical and dynamical properties of asteroid families. in: *Asteroids III* (W.F. Bottke, A. Cellino, P. Paolicchi and R.P. Binzel, Eds.), pp. 619–631. Arizona University Press, Tucson.

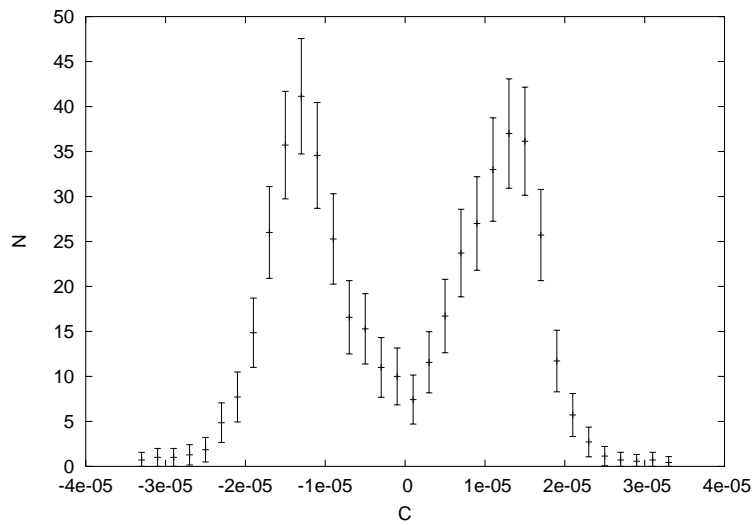


Fig. 1.— Symbols show number  $N_{\text{obs}}(C)$  of observed Erigone members in  $(C, C + \Delta C)$  bins with error-bars given as  $\sqrt{N_{\text{obs}}(C)}$ . We chose  $\Delta C = 2 \times 10^{-6}$  AU and  $a_c$  uniformly averaged in the range (2.368, 2.374) AU. Though not perfect  $N_{\text{obs}}(C)$  is approximately symmetric about  $C = 0$  with significant maxima at  $C = \pm 1.5 \times 10^{-5}$  AU.

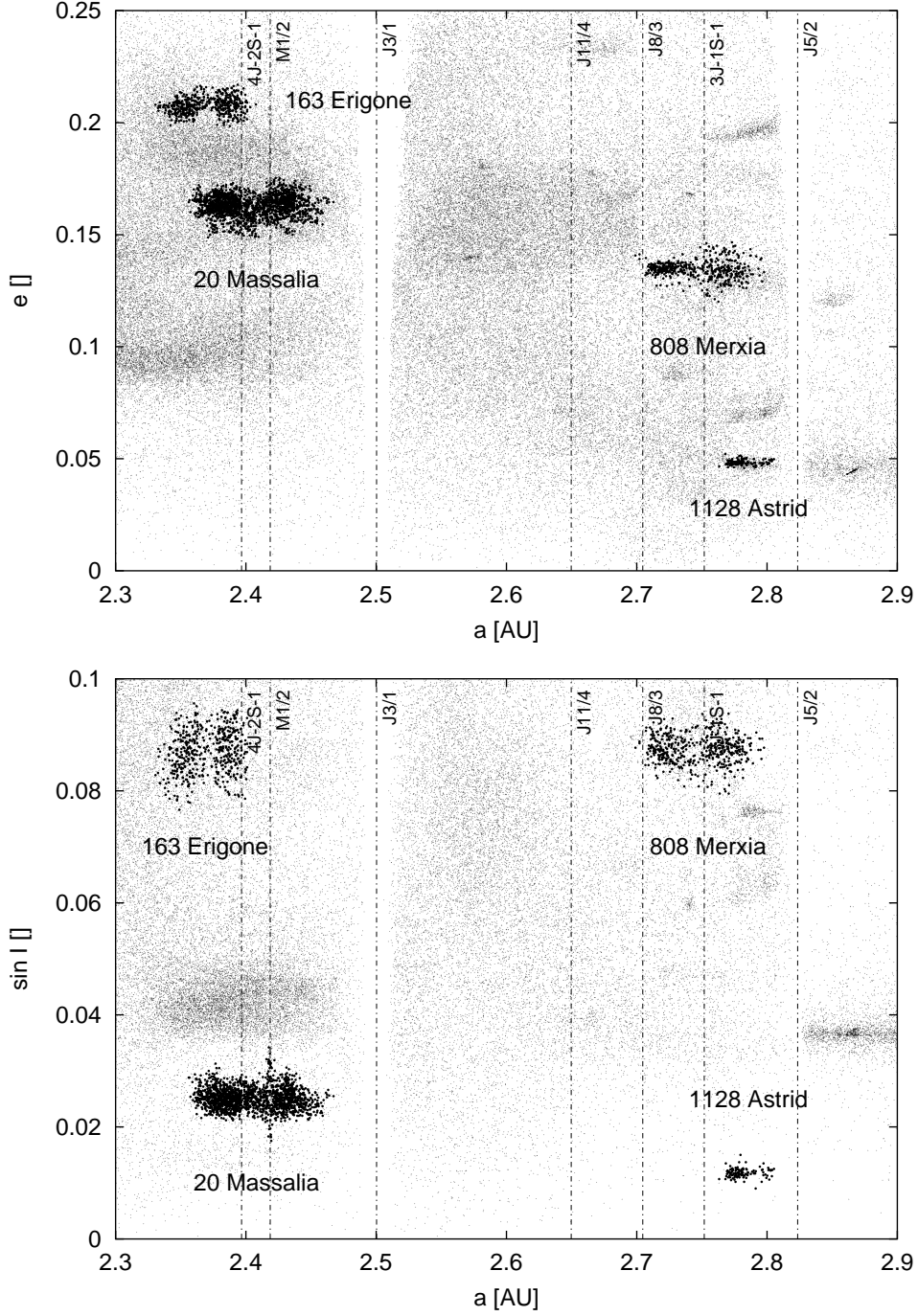


Fig. 2.— Four prominent families that show concentrations of asteroids at extreme value of semimajor axis: Erigone, Massalia, Merxia and Astrid. Here we show their nominal realizations (see the text) in the space of proper orbital elements: (i) semimajor axis  $a$  vs. eccentricity  $e$  – top, and (ii) semimajor axis  $a$  vs. sine of inclination  $\sin I$  – bottom. We also indicate position of the major mean motion resonances with Jupiter (J3/1, J5/2, J8/3) and some of the weaker resonances (e.g. M1/2, 3J–1S–1 or 4J–2S–1). Dots are all background asteroids and other families not considered in this paper.

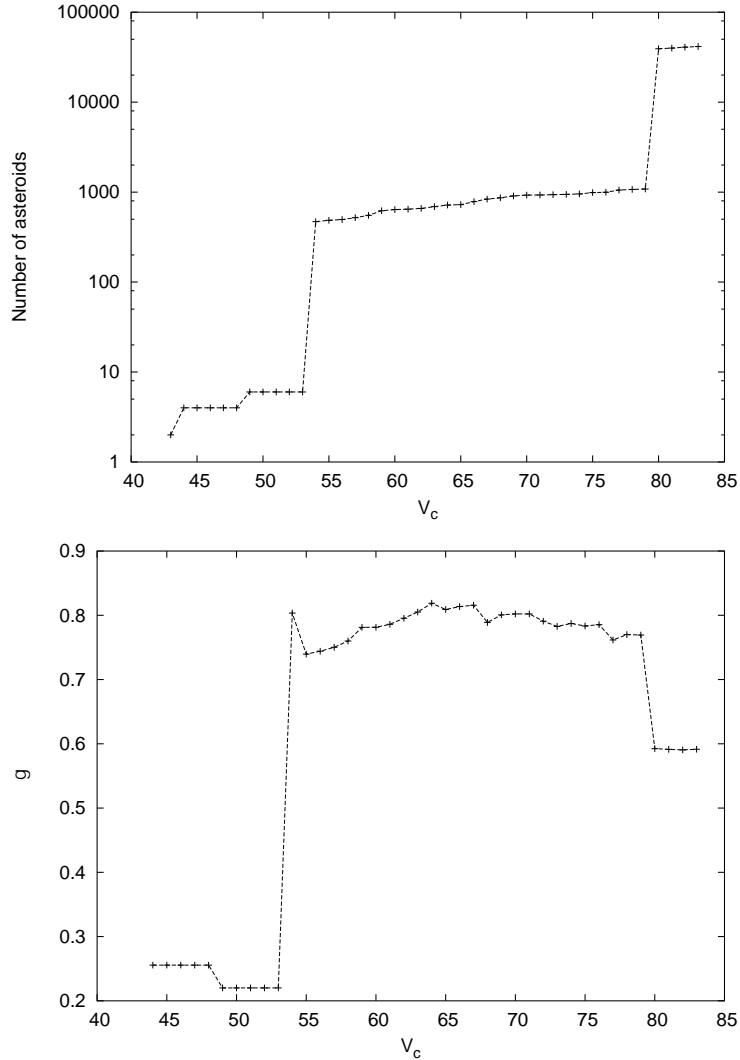


Fig. 3.— Number of asteroids associated with Erigone family (top) and power-law index  $\gamma$  of the cumulative magnitude distribution in the range (13.5, 15.5) (bottom) as a function of the HCM cut-off velocity  $V_c$ . Two critical values of  $V_c$  are: (i) 54 m/s, when the close vicinity of (163) Erigone merges with the remaining part of the family, and (ii) 80 m/s, when the family (as formally identified with the HCM method) coalesces with bulk of the inner main belt. The family is reasonably well defined in between those two  $V_c$  values, slowly accumulating outskirts members and interlopers. In this interval,  $\gamma$  consistently oscillates between 0.74 and 0.8. When the bulk of the inner main belt formally associates with the family,  $\gamma$  acquires a value close to 0.6 (determined also by Ivezić et al. (2001) from the SDSS data).

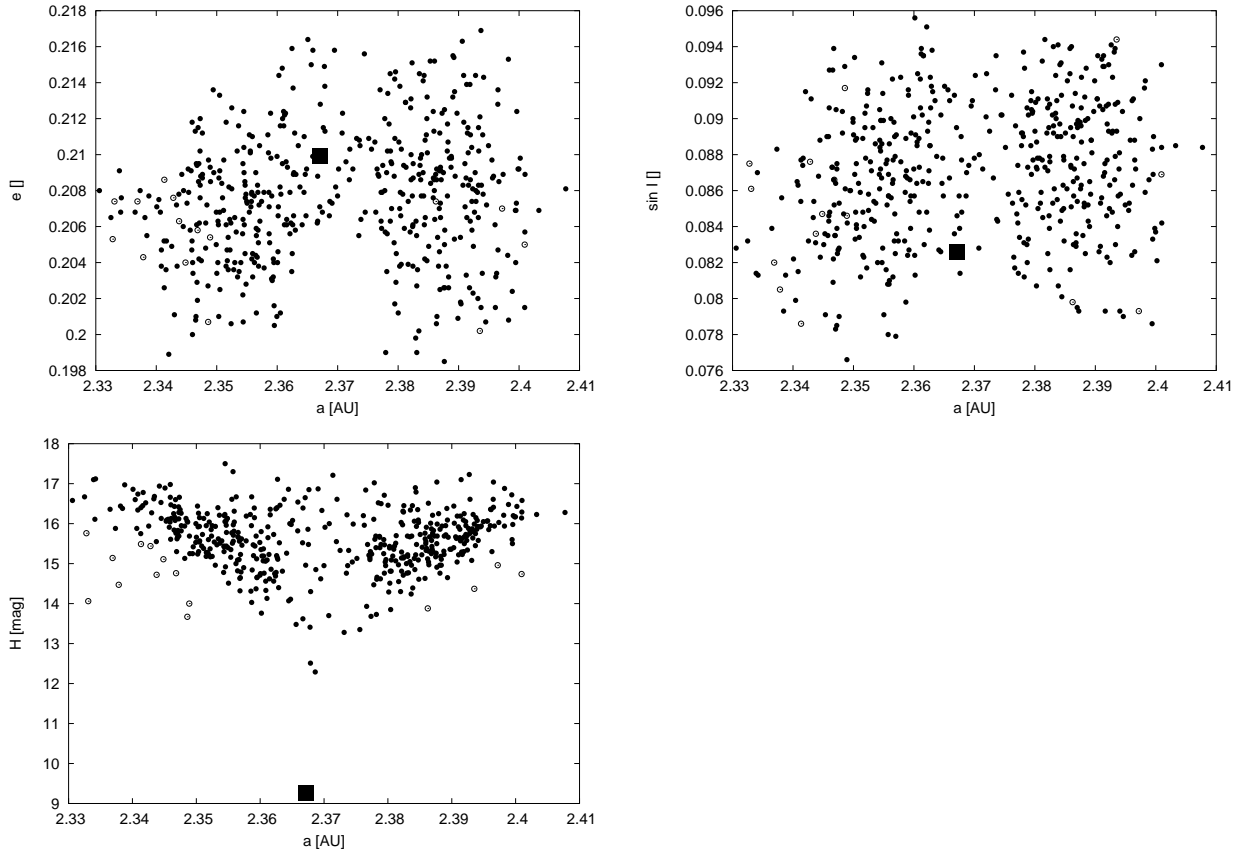


Fig. 4.— Erigone family at HCM velocity 56 m/s projected onto a plane of proper semimajor axis  $a$  vs. proper eccentricity  $e$  (top and left), proper semimajor axis  $a$  vs. proper sine of inclination  $\sin I$  (top and right), proper semimajor axis  $a$  vs. absolute magnitude  $H$  (bottom and left); (163) Erigone is shown as a large filled square. Suspected interlopers are open circles. About half of these open circles at  $a \leq 2.35$  AU is recognized alien to the family using the SDSS PC1-PC<sub>2</sub> clustering (Sec. 3.5).

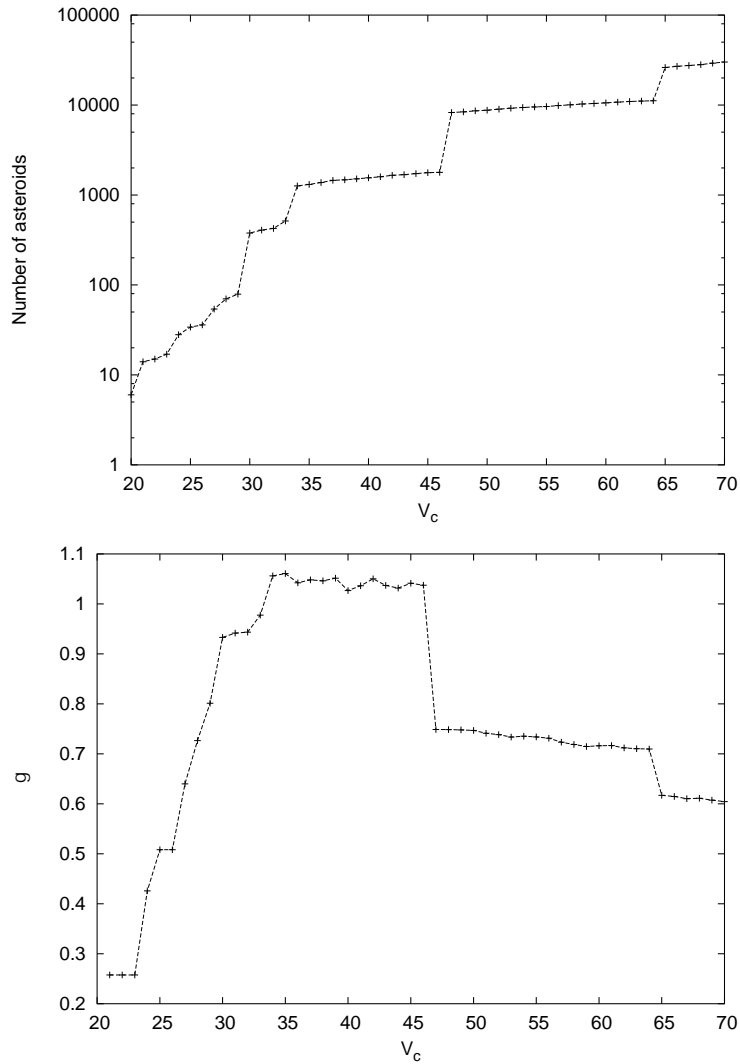


Fig. 5.— The same as in Fig. 3 but for Massalia family. Critical transitions occur for  $V_c = 47$  m/s, for which the family accumulates surrounding main-belt asteroids, and 64 m/s, when basically all inner main belt asteroids coalesces with the family. The transition at  $V_c = 34$  m/s has to do with associating all left side of the family (for which  $a \leq 2.405$  AU) and only for that value the family is assumed to be complete. In between 34 m/s and 46 m/s the number of the family members only slightly increases and its  $\gamma$  slope remains extremely high ( $\approx 1.03$ ).

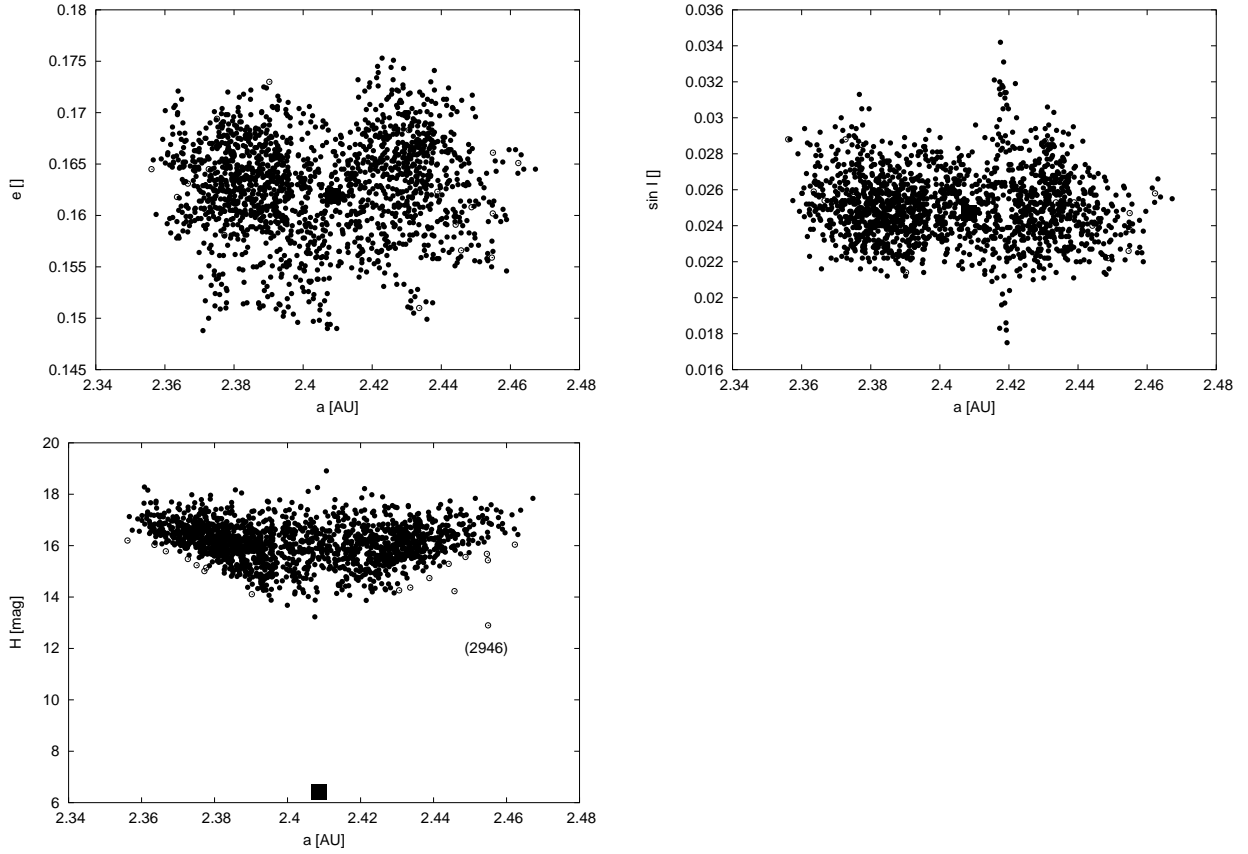


Fig. 6.— Massalia family at HCM velocity 44 m/s projected onto a plane of proper semimajor axis  $a$  vs. proper eccentricity  $e$  (top and left), proper semimajor axis  $a$  vs. proper sine of inclination  $\sin I$  (top and right), proper semimajor axis  $a$  vs. absolute magnitude  $H$  (bottom and left); the asteroid (20) Massalia is shown as a large filled square. Suspected interlopers are open circles; the asteroid (2946) Muchachos is a spectrally confirmed interloper. Some of the weak mean motion resonances are shown:  $M1/2$ , an exterior resonance with Mars, produces the prominent spread of the inclination at  $a \simeq 2.42$  AU,  $4J-2S-1$ , a three-body resonance, may be responsible for the larger scatter of eccentricity below  $a \simeq 2.41$  AU (Sec. 5.2 and Fig. 24).

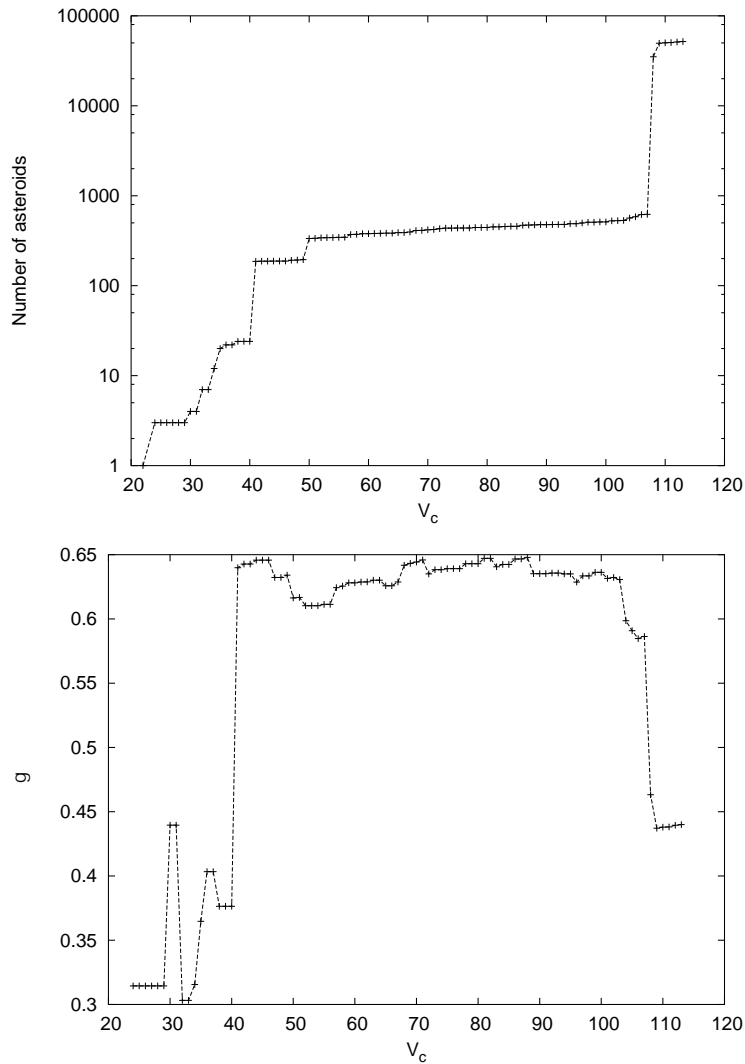


Fig. 7.— The same as in Fig. 3 but for Merxia family. A critical transition occurs at  $V_c = 108$  m/s, when the formal family coalesces with a fair portion of the middle and outer parts of the main asteroid belt. Two “internal” transitions occur at  $V_c = 41$  m/s, when the whole left part of the family associates with the nearest surrounding of (808) Merxia, and at  $V_c = 50$  m/s, when also the right part of the family (for which  $a \geq 2.75$  AU) associates with the family. Until the coalescence with the bulk of asteroid belt, the family’s  $\gamma$  parameter is consistently high in between the 0.62 and 0.65 values.

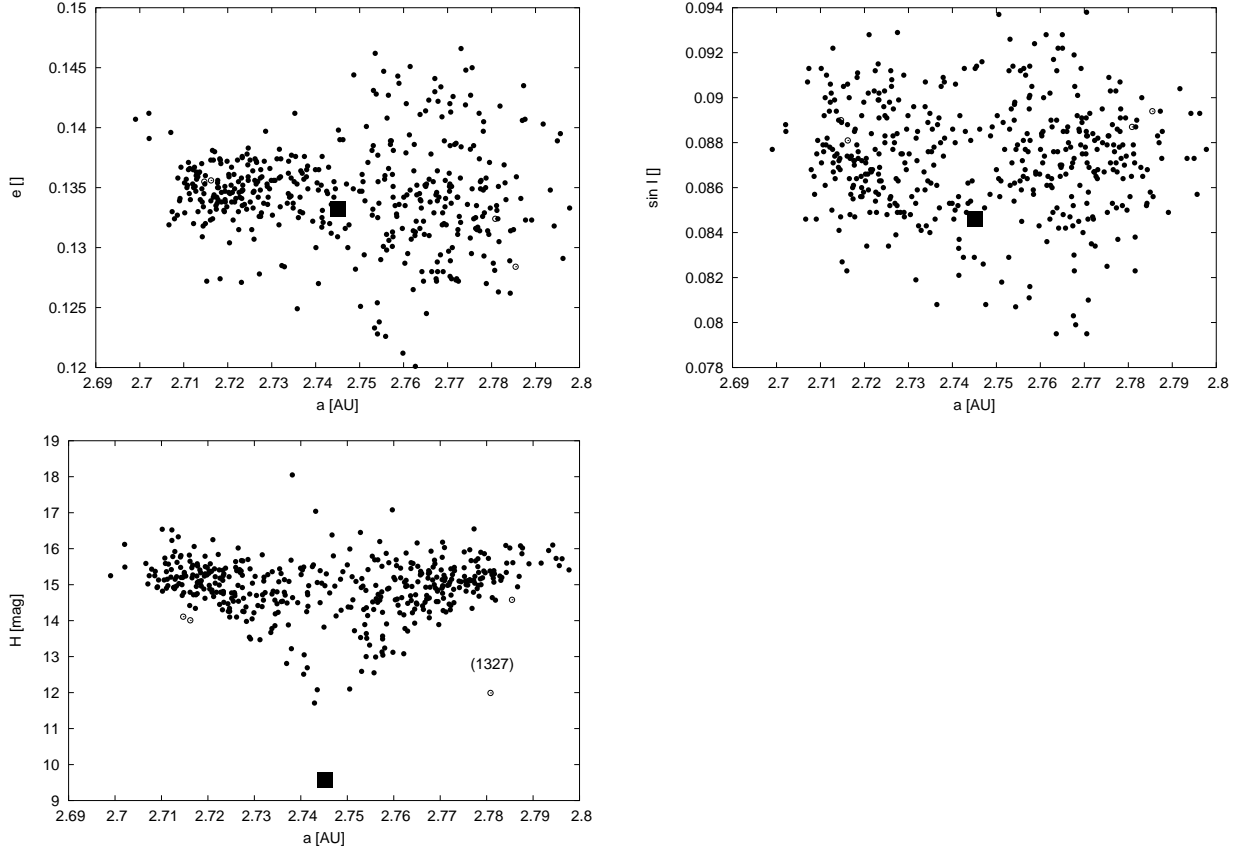


Fig. 8.— Merxia family at HCM velocity 80 m/s projected onto a plane of proper semimajor axis  $a$  vs. proper eccentricity  $e$  (top and left), proper semimajor axis  $a$  vs. proper sine of inclination  $\sin I$  (top and right), proper semimajor axis  $a$  vs. absolute magnitude  $H$  (bottom and left); the asteroid (808) Merxia is shown as a large filled square. Suspected interlopers are open circles; asteroid (1327) Namaqua is a spectrally recognized interloper. Some of the weak mean motion resonances are shown: 3J–1S–1, a three-body resonance, is likely responsible for the large scatter of proper eccentricities for  $a \geq 2.75$  AU (Sec. 5.3 and Fig. 25).

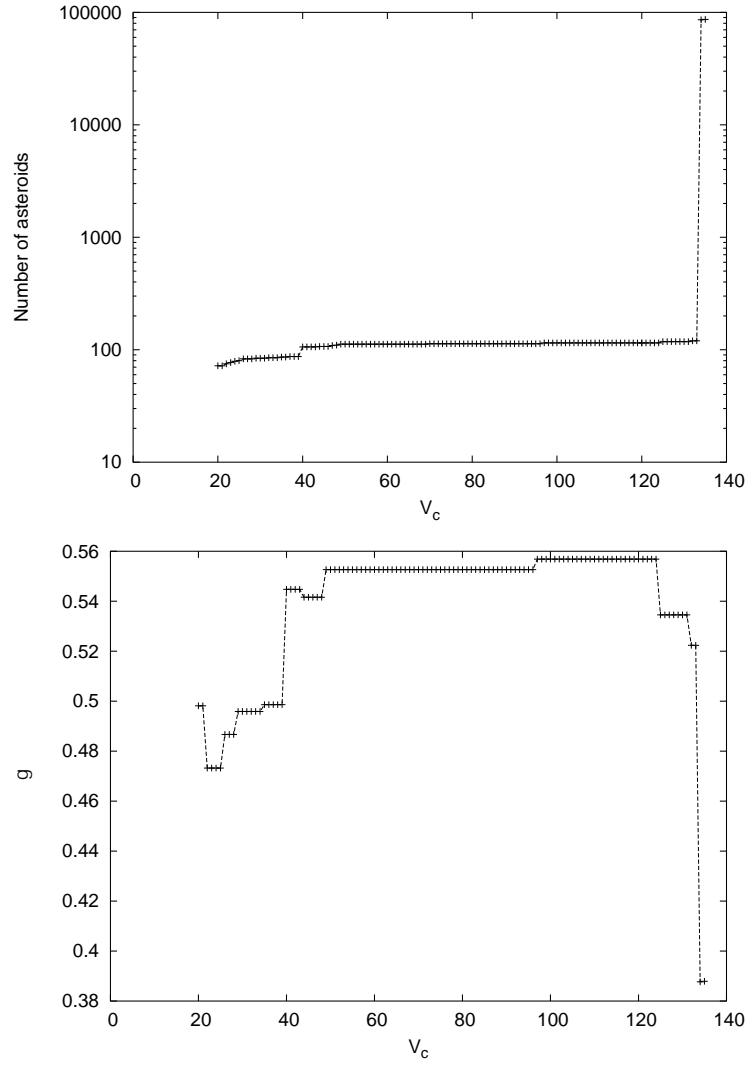


Fig. 9.— The same as in Fig. 3 but for Astrid family. The family shows only a weak dependence on the HCM velocity cut-off  $V_c$  at the abscissa until a critical value of 133 m/s, when the family coalesces with the surrounding zone of the main belt.

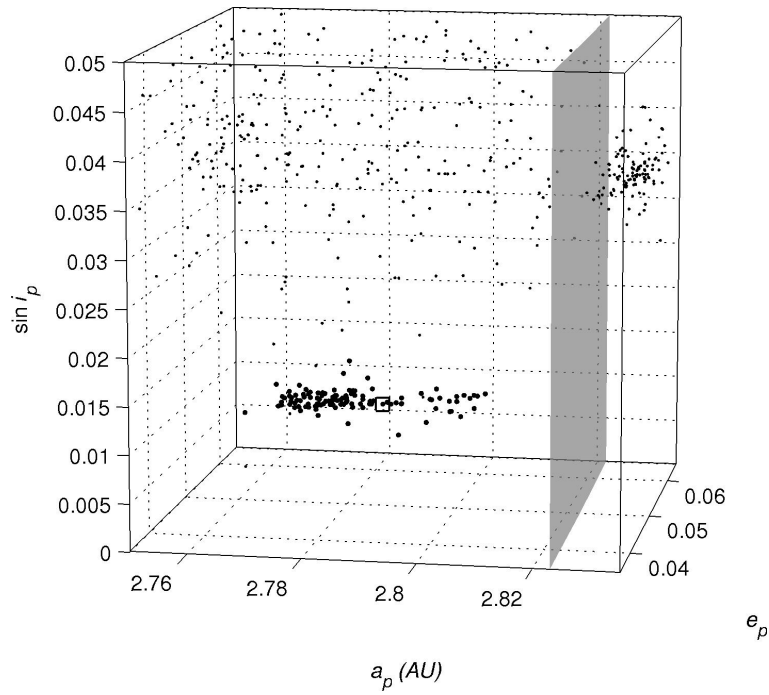


Fig. 10.— Astrid family (bold symbols) at HCM velocity 70 m/s shown here as a cluster in the three-dimensional space of proper orbital elements; (1128) Astrid is indicated by the open square. Background asteroids are shown as dots (the clump above the J5/2 resonance is a tail of the Koronis family). This view allows to discover that a zone between the family termination at  $a \sim 2.81$  AU and separatrix of the J5/2 mean motion resonance at  $a \sim 2.82$  AU (shaded plane) is entirely void of any objects.

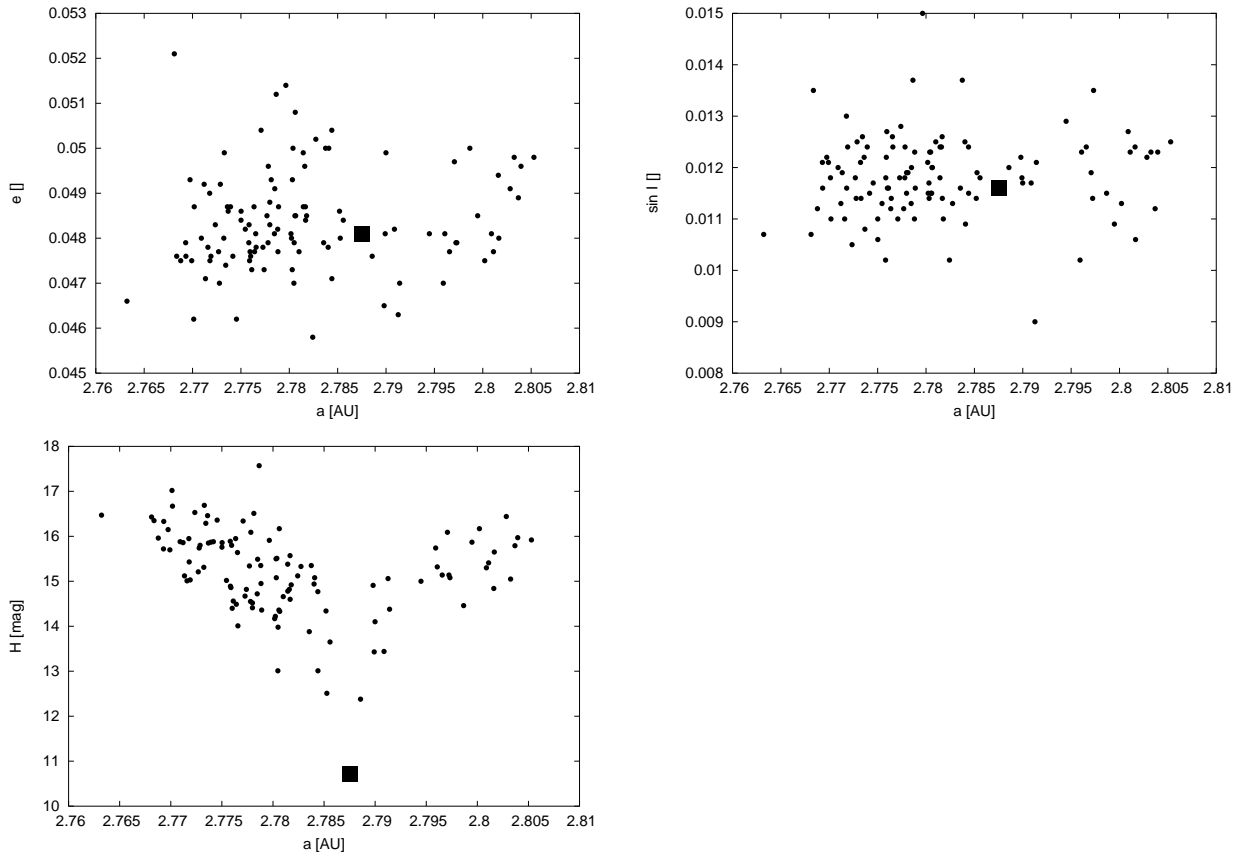


Fig. 11.— Astrid family at HCM velocity 70 m/s projected onto a plane of proper semimajor axis  $a$  vs. proper eccentricity  $e$  (top and left), proper semimajor axis  $a$  vs. proper sine of inclination  $\sin I$  (top and right), proper semimajor axis  $a$  vs. absolute magnitude  $H$  (bottom and left); (1128) Astrid is shown as a filled square.

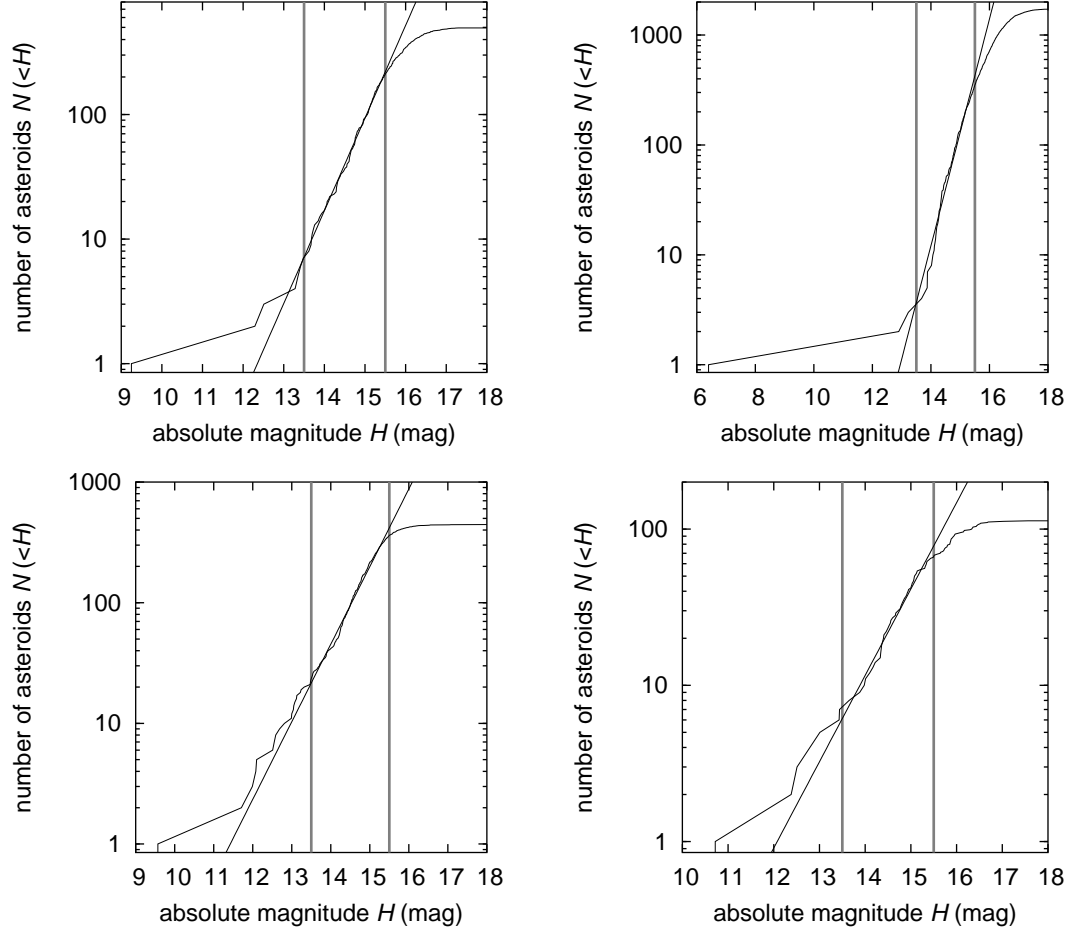


Fig. 12.— The cumulative distributions  $N(< H)$  for: (i) Erigone – top and left, (ii) Massalia – top and right, (iii) Merxia – bottom and left, and (iv) Astrid – bottom and right; nominal families shown here. We use  $N(< H) \propto 10^{\gamma H}$  approximation in the magnitude range (13.5, 15.5) and obtain the following values of the  $\gamma$  parameter: (i)  $\gamma = 0.74$  for Erigone, (ii)  $\gamma = 1.03$  for Massalia, (iii)  $\gamma = 0.64$  for Merxia, and (iv)  $\gamma = 0.55$  for Astrid. The exponent  $\beta$  of the power-law approximation of the cumulative size distribution is related to  $\gamma$  as  $\beta = -5\gamma$ . Except for the Astrid family, the magnitude distribution is much steeper than the collisionally evolved system for which Dohnanyi (1969) derived  $\gamma_{\text{Doh}} = 0.5$  or  $\beta_{\text{Doh}} = -2.5$ .

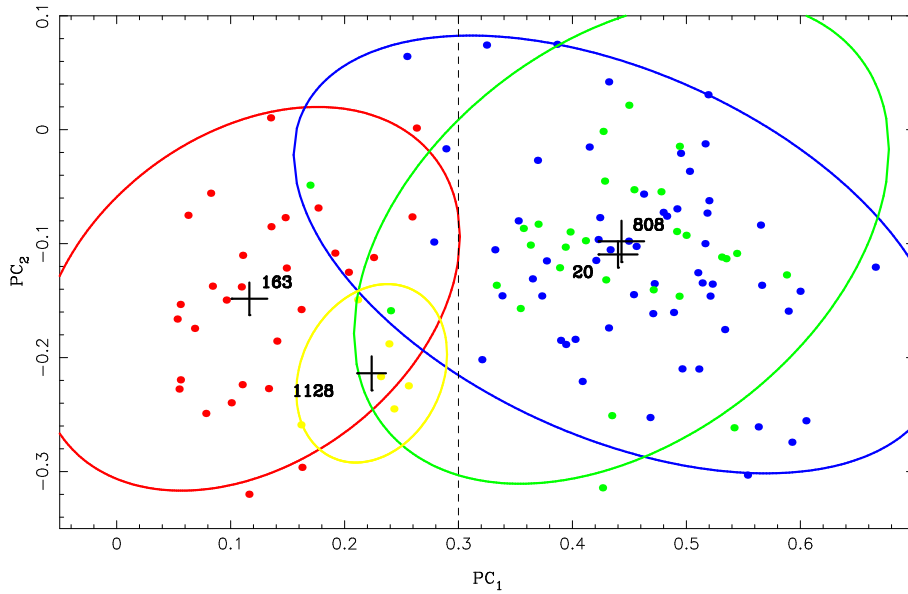


Fig. 13.— Principal spectral components  $PC_1$  and  $PC_2$  derived for members of our studied families from the Sloan Sky Digital Survey (SDSS; data release 3). Dots are data for individual asteroids: Erigone members (red), Astrid members (yellow), Massalia members (blue), and Merxia members (green). The black crosses are mean values in the corresponding family with standard errors; labels are the number of leading asteroid in the family. The dashed vertical line at  $PC_1 = 0.3$  roughly divides this parametric space to C (left) and S (right) complexes (e.g. Binzel and Bus, 2002; Nesvorný et al., 2005). The ellipses show 90% confidence level boundaries of membership for each of the families based on the available SDSS data.

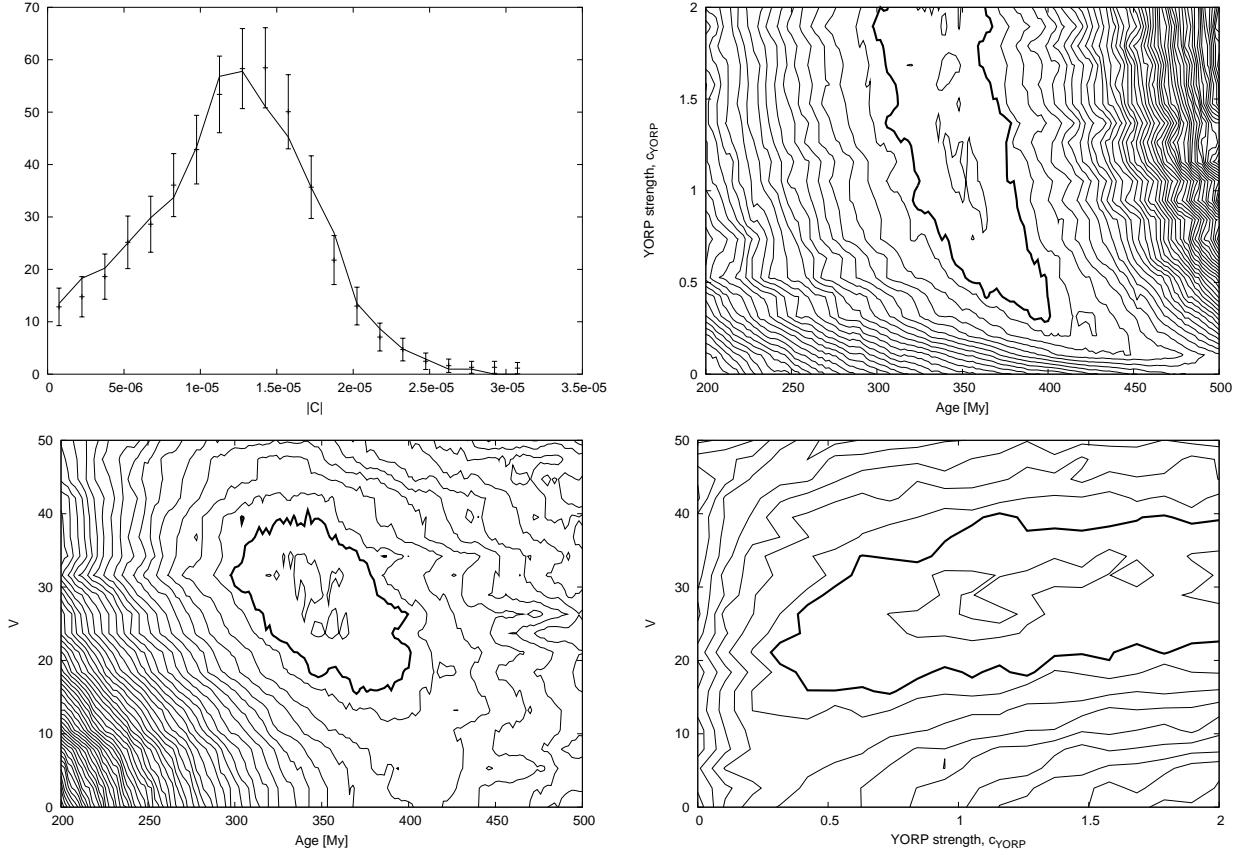


Fig. 14.— Results of our simulation for the Erigone family with mean albedo  $p_V = 0.05$  and surface thermal conductivity  $K = 0.05$  W/m/K. The best-fit solution  $N(C)$  (solid line) over-imposed over data points  $N_{\text{obs}}(C)$  (intervals) – top and left;  $N(C)$  is symmetric about  $C > 0$  and in our analysis we folded asteroids with  $C < 0$  into the corresponding bin with  $C > 0$ . Top and right, and bottom figures show projection of the best value of the target function  $\Psi_{\Delta C}$  for various pairs of the solved-for parameters: (i) age  $T$  vs. YORP strength parameter  $c_{\text{YORP}}$ , (ii) age  $T$  vs. characteristic velocity  $V$  of initial ejection of  $D = 5$  km fragments, and (iii)  $c_{\text{YORP}}$  vs.  $V$ . Formally  $1\sigma$  contour, defined by  $\Psi_{\Delta C} = 21$ , is shown in bold; contours for other values of the target function are shown in light.

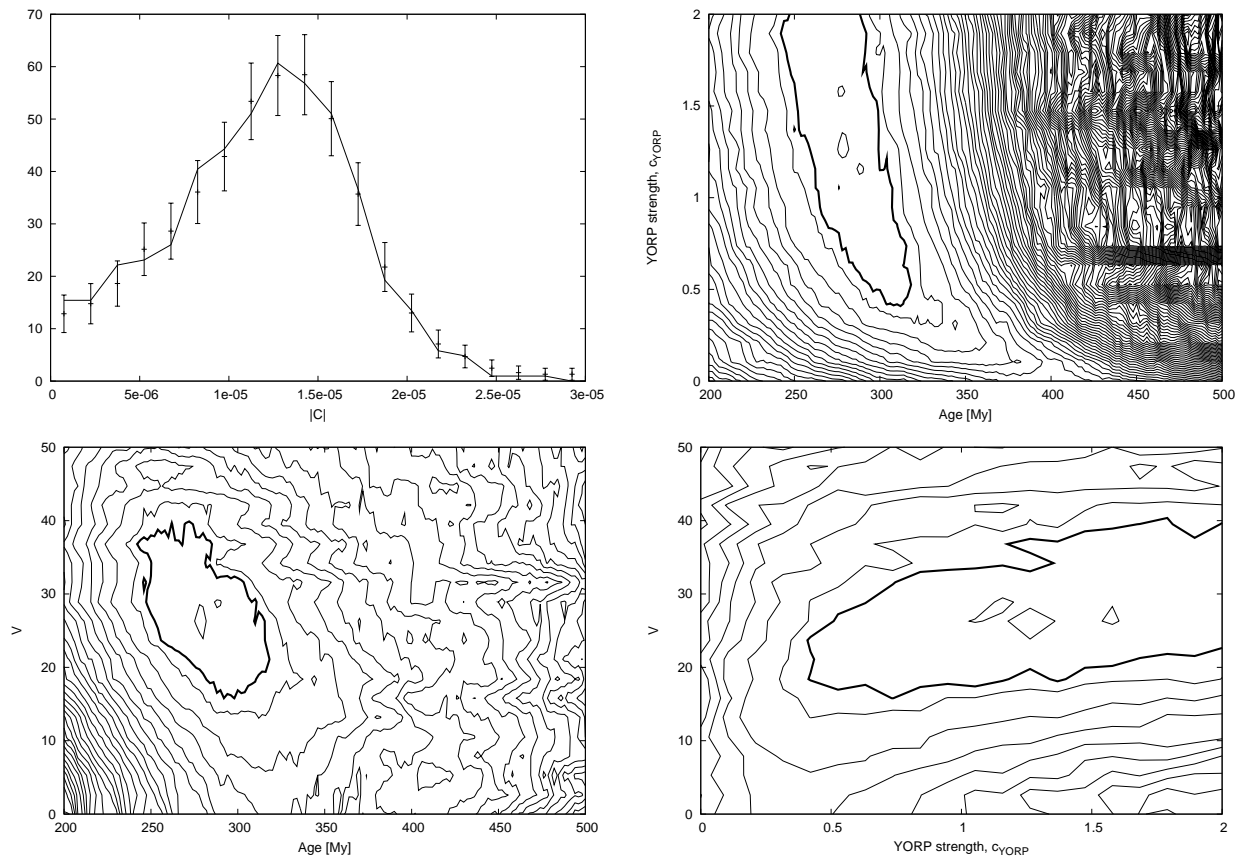


Fig. 15.— The same as in Fig. 14 but assuming the surface thermal conductivity uniformly spans interval  $K = 0.005 - 0.05$  W/m/K.

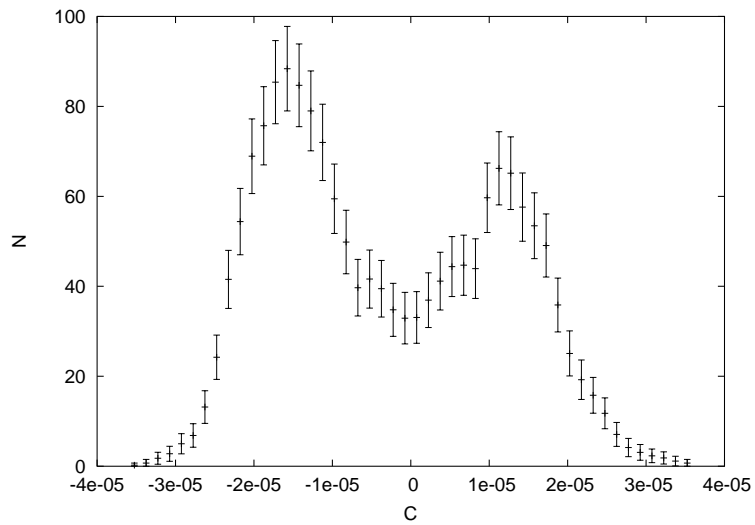


Fig. 16.— Symbols show number  $N_{\text{obs}}(C)$  of observed Massalia members in  $(C, C + \Delta C)$  bins with error-bars given as  $\sqrt{N_{\text{obs}}(C)}$ . We chose  $\Delta C = 1.5 \times 10^{-6}$  AU and  $a_c$  uniformly averaged in the range (2.407, 2.414) AU. In this case,  $N(C)$  is not symmetric about  $C = 0$ , but the number of asteroids for positive  $C$  is systematically smaller. We suggest this is an effect of partial leakage of objects from the family along the exterior Martian resonance M1/2. We thus decided to discard  $C > 0$  distribution from our analysis and use only  $N(C)$  for  $C < 0$ .

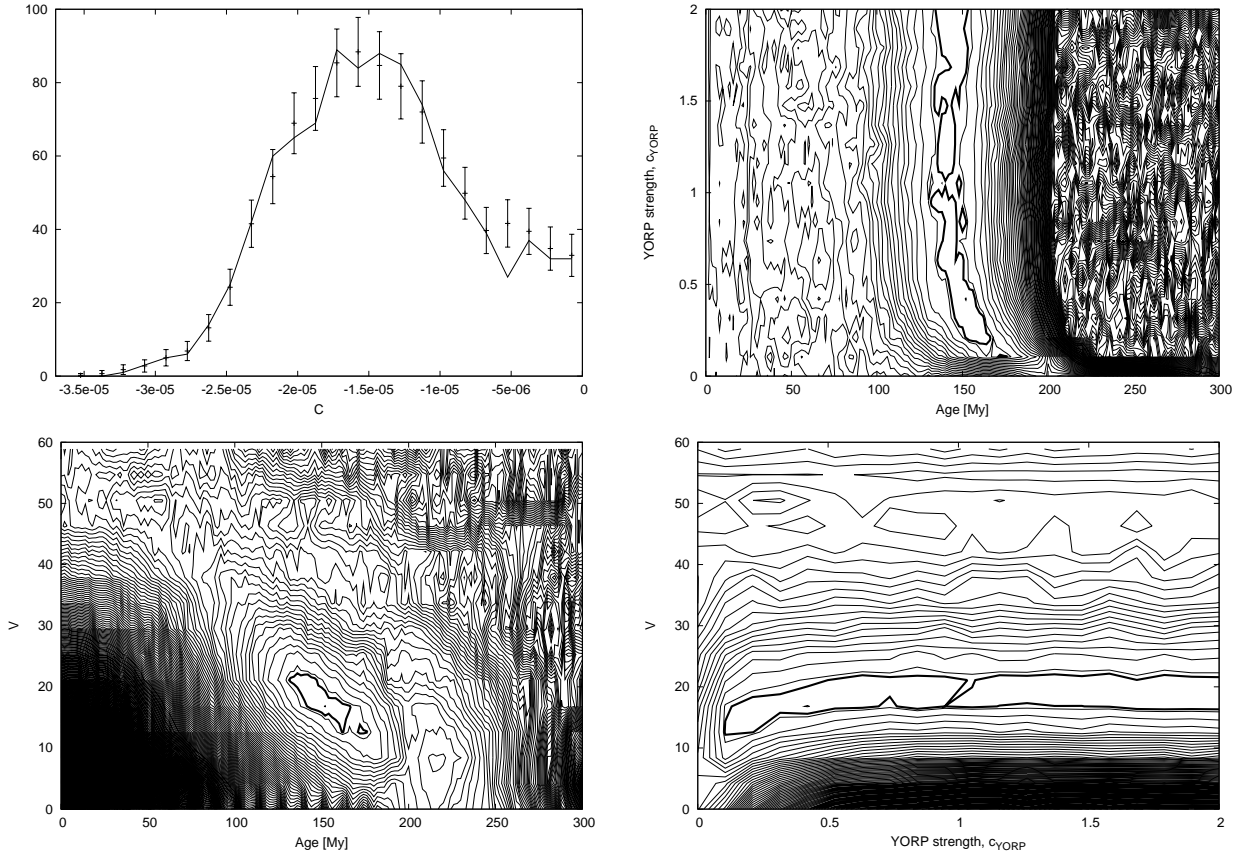


Fig. 17.— Results of our simulation for the Massalia family with mean albedo  $p_V = 0.21$  and surface thermal conductivity  $K = 0.005$  W/m/K. Top and left is the best-fit simulation of number of asteroids  $N(C)$  in the  $C$ -bins (solid line) compared to the observed family  $N_{\text{obs}}(C)$  (symbols and error-bars). Top and right, and bottom figures show projection of the best value of the target function  $\Psi_{\Delta C}$  for various pairs of the solved-for parameters: (i) age  $T$  vs. YORP strength parameter  $c_{\text{YORP}}$ , (ii) age  $T$  vs. characteristic velocity  $V$  of initial ejection of  $D = 5$  km fragments, and (iii)  $c_{\text{YORP}}$  vs.  $V$ . Formally  $1\sigma$  contour, defined by  $\Psi_{\Delta C} = 24$ , is shown in bold; contours for other values of the target function are shown in light.

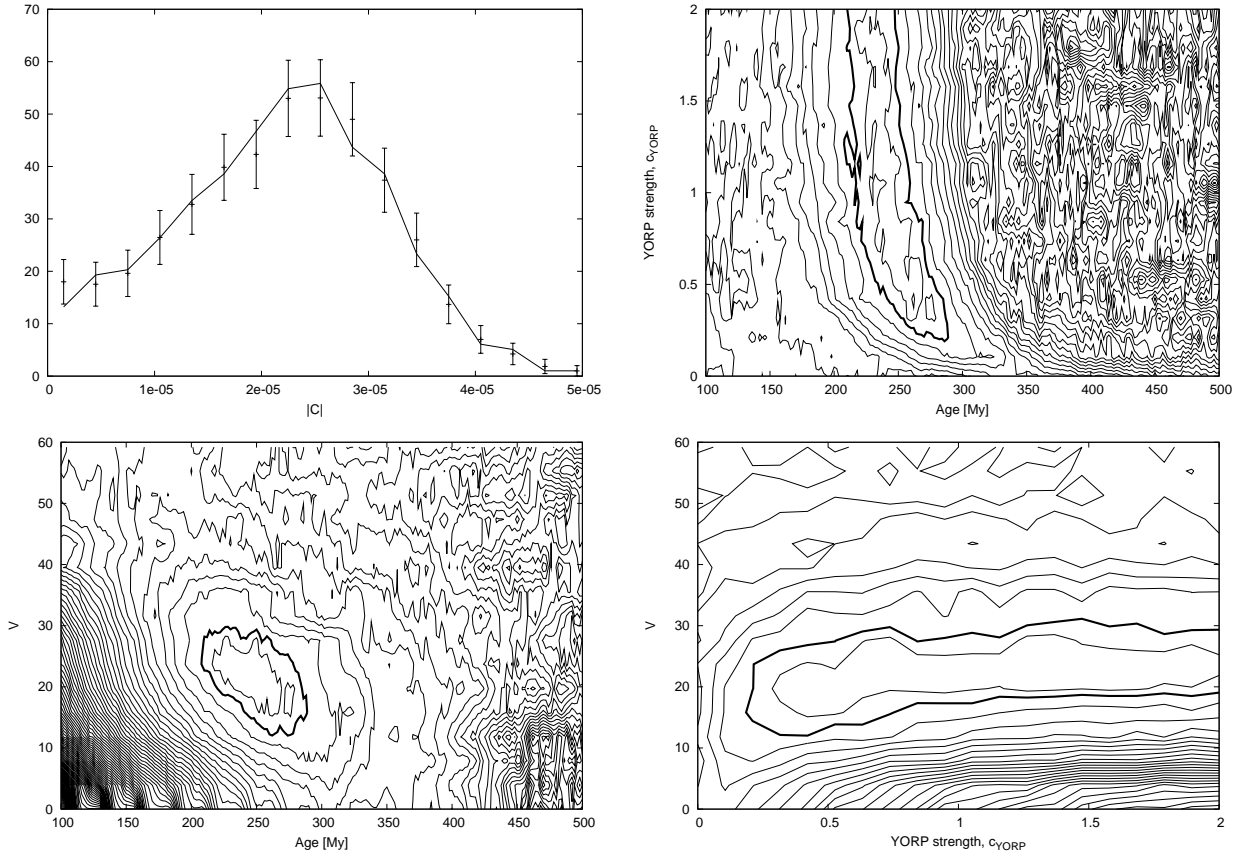


Fig. 18.— Results of our simulation for the Merxia family with mean albedo  $p_V = 0.22$  and surface thermal conductivity  $K = 0.005$  W/m/K. Top and left is the best-fit simulation of number of asteroids  $N(C)$  in the  $C$ -bins (solid line) compared to the observed family  $N_{\text{obs}}(C)$  (symbols and error-bars). Top and right, and bottom figures show projection of the best value of the target function  $\Psi_{\Delta C}$  for various pairs of the solved-for parameters: (i) age  $T$  vs. YORP strength parameter  $c_{\text{YORP}}$ , (ii) age  $T$  vs. characteristic velocity  $V$  of initial ejection of  $D = 5$  km fragments, and (iii)  $c_{\text{YORP}}$  vs.  $V$ . Formally  $1\sigma$  contour, defined by  $\Psi_{\Delta C} = 17$ , is shown in bold; contours for other values of the target function are shown in light.

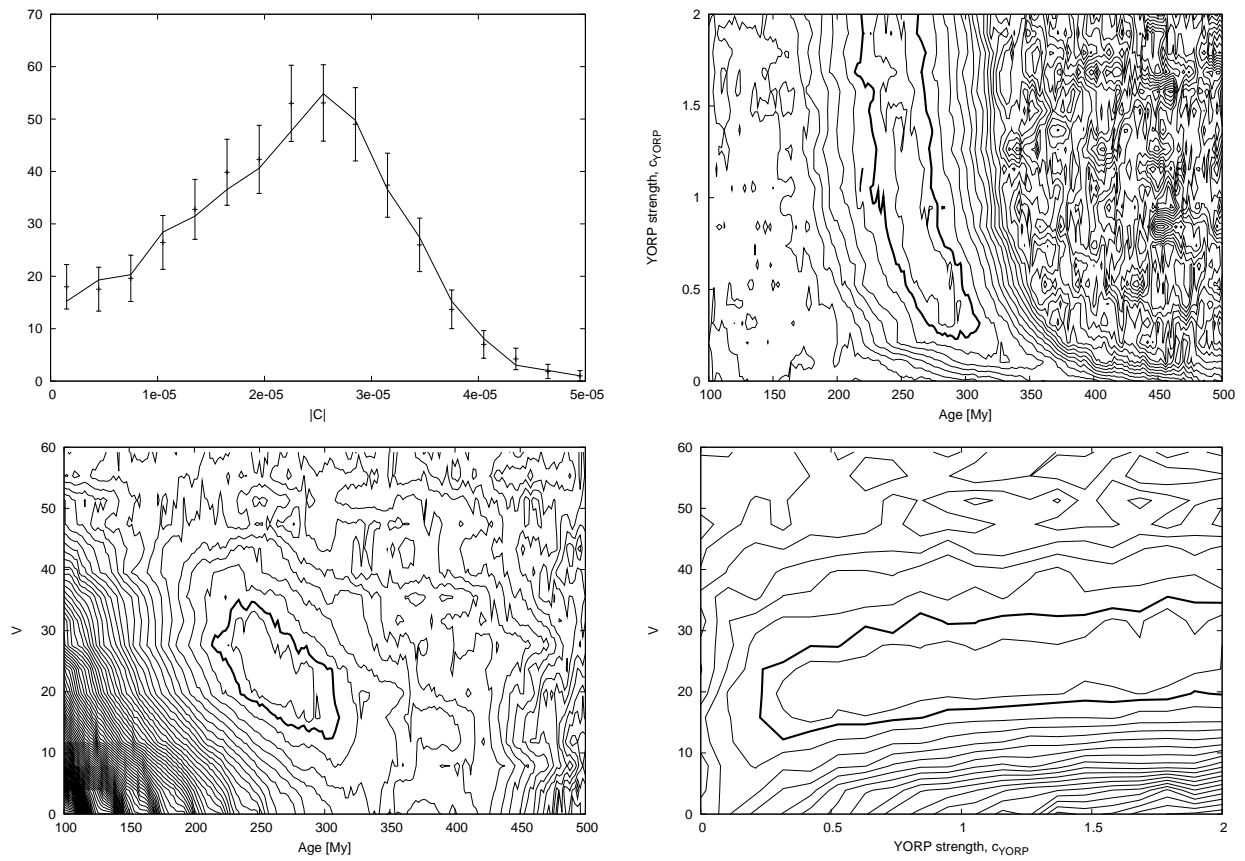


Fig. 19.— The same as in Fig. 18 but now assuming mean albedo  $p_V = 0.20$  and surface thermal conductivity randomly spanning  $0.001 - 0.01$  W/m/K values.

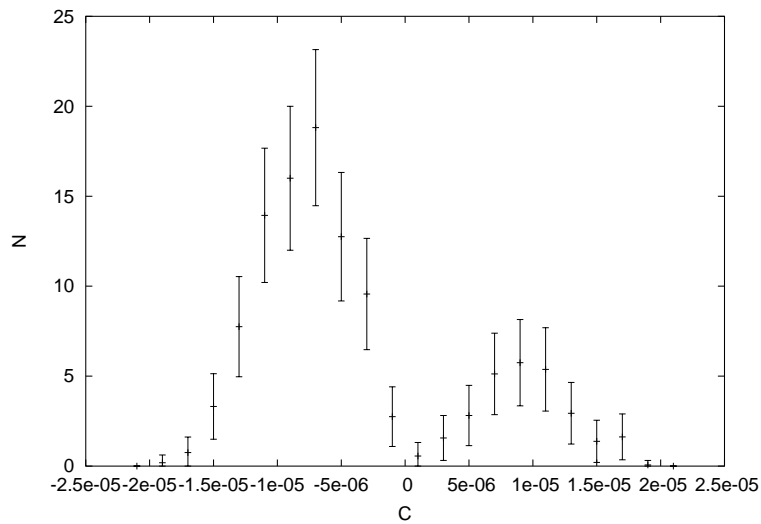


Fig. 20.— Symbols show number  $N_{\text{obs}}(C)$  of observed Astrid members in  $(C, C + \Delta C)$  bins with error-bars given as  $\sqrt{N_{\text{obs}}(C)}$ . We chose  $\Delta C = 2 \times 10^{-6}$  AU and  $a_c$  uniformly averaged in the range  $(2.785, 2.788)$  AU. In this case,  $N(C)$  is not symmetric about  $C = 0$ , with number of asteroids for positive  $C$  systematically smaller. In Sec. 5.4 we consider possibilities for this asymmetry and in the further analysis we use the  $C < 0$  part of the data only.

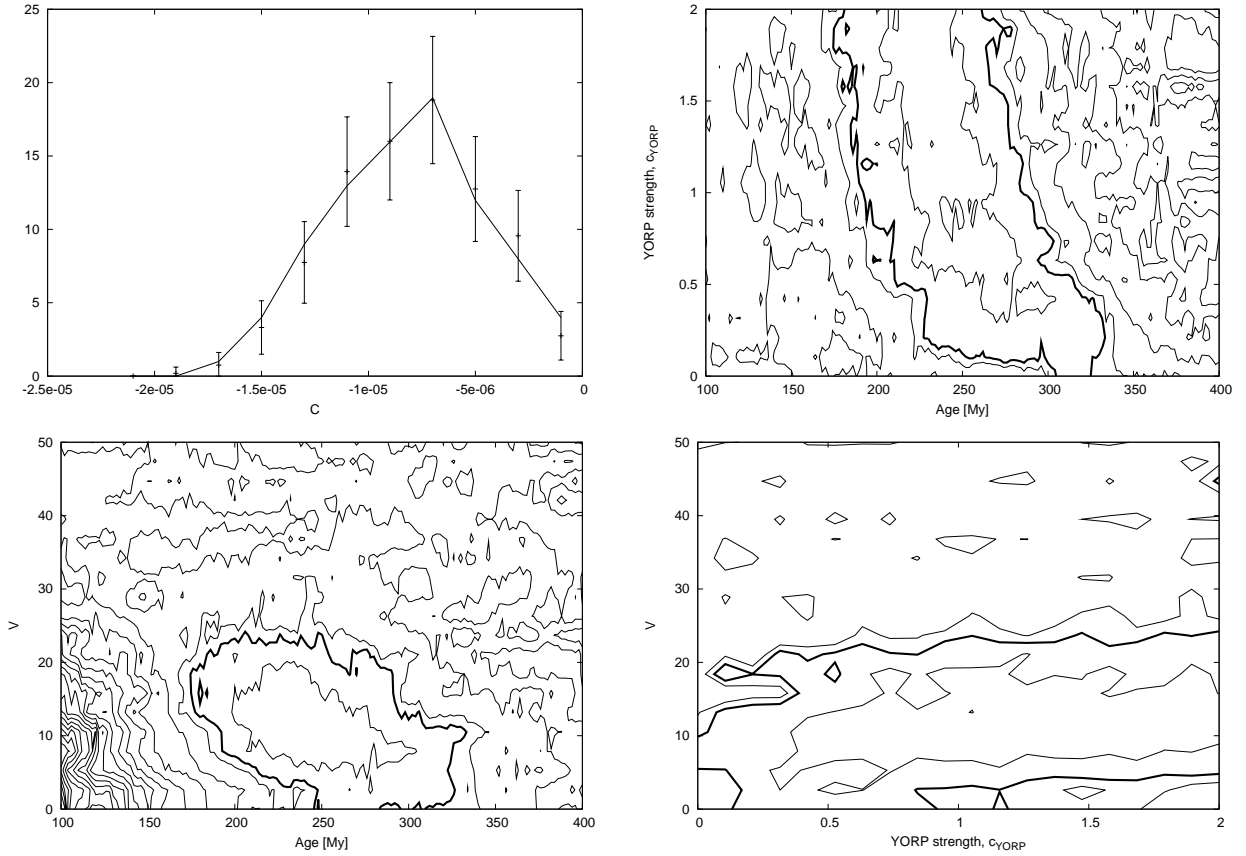


Fig. 21.— Results of our simulation for the Astrid family with mean albedo  $p_V = 0.08$  and surface thermal conductivity  $K = 0.05$  W/m/K. Top and left is the best-fit simulation of number of asteroids  $N(C)$  in the  $C$ -bins (solid line) compared to the observed family  $N_{\text{obs}}(C)$  (symbols and error-bars). Top and right, and bottom figures show projection of the best value of the target function  $\Psi_{\Delta C}$  for various pairs of the solved-for parameters: (i) age  $T$  vs. YORP strength parameter  $c_{\text{YORP}}$ , (ii) age  $T$  vs. characteristic velocity  $V$  of initial ejection of  $D = 5$  km fragments, and (iii)  $c_{\text{YORP}}$  vs.  $V$ . Formally  $1\sigma$  contour, defined by  $\Psi_{\Delta C} = 11$ , is shown in bold; contours for other values of the target function are shown in light.

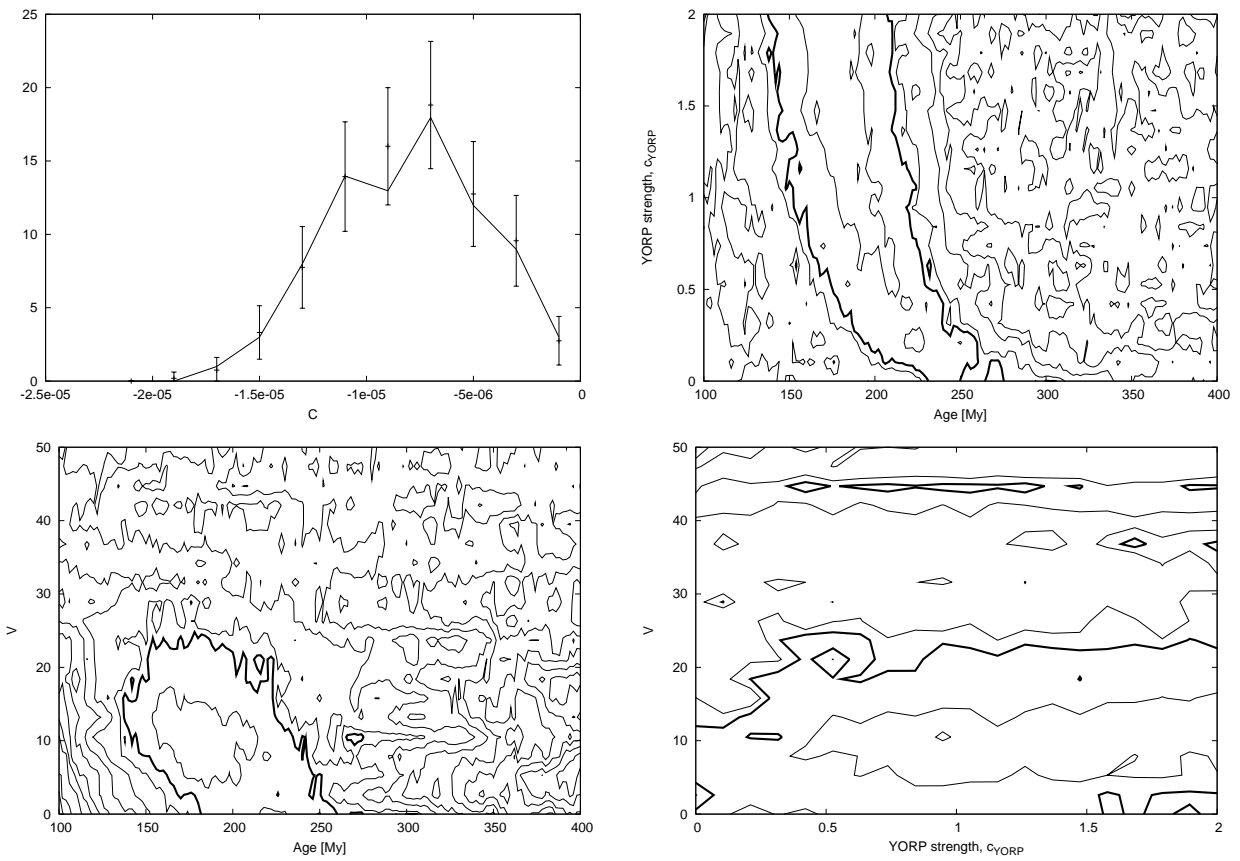


Fig. 22.— The same as in Fig. 21 but now assuming mean albedo surface thermal conductivity randomly spanning 0.005 – 0.05 W/m/K values.

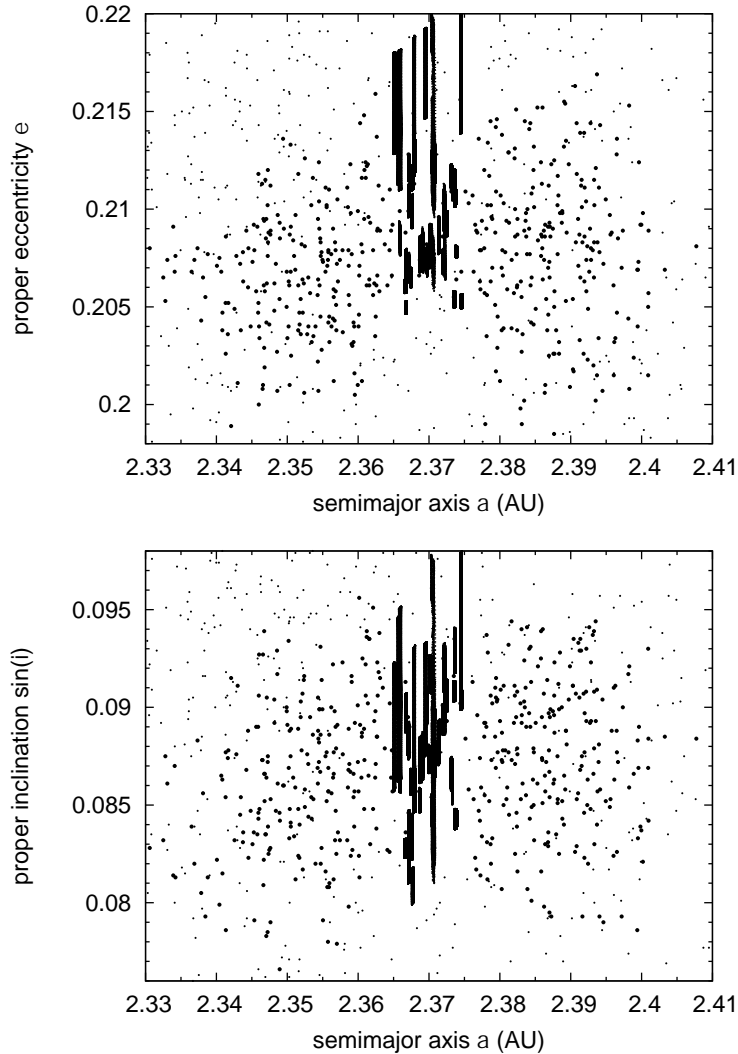


Fig. 23.— Evolution tracks of a sample of numerically integrated orbits without Yarkovsky forces in the Erigone family: (i) proper semimajor axis  $a$  vs proper eccentricity  $e$  (top), and (ii) proper semimajor axis  $a$  vs proper sine of inclination  $\sin I$  (bottom). Initial data of 108 selected real members, and their close clones, chosen near the center of the family, where depletion is observed. Integration timespan has been set to 500 My, more than the estimated age of the family from Figs. 14 and 15. The orbits are stable indicating no macroscopic chaos that could be associated with any of the weak mean motion resonances. The larger observed variations in proper eccentricity and inclination is due to interaction with the  $z_2$  secular resonance. This effect is however very stable on a long-term. As a result, the observed depletion is unlikely to be explained by chaotic leakage from the central zone in the family, rather it follows from synergy of the Yarkovsky/YORP evolution discussed earlier in this paper.

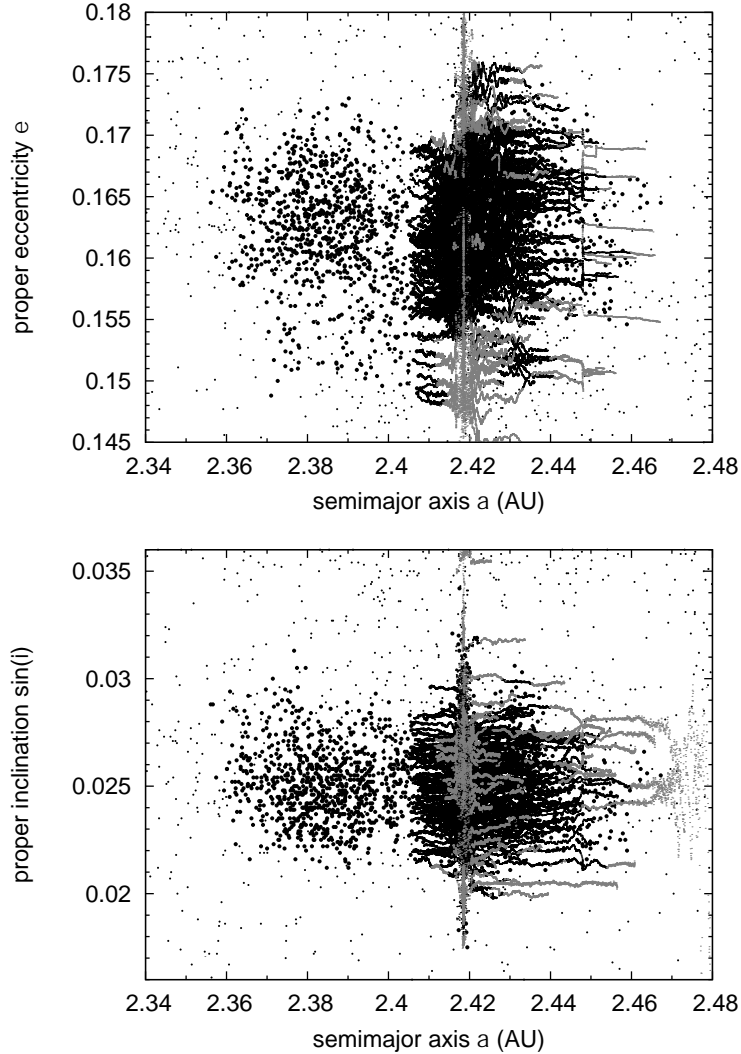


Fig. 24.— Evolution tracks of a sample of numerically integrated orbits with Yarkovsky forces in the Massalia family: (i) proper semimajor axis  $a$  vs proper eccentricity  $e$  (top), and (ii) proper semimajor axis  $a$  vs proper sine of inclination  $\sin I$  (bottom). Initial data of 137 selected real members chosen near the center of the family. Obliquities, roughly set to  $45^\circ$ , make the bodies migrate toward larger values of the semimajor axis. Upon reaching the position of the exterior M1/2 mean motion resonance with Mars, the proper  $e$  and proper  $\sin I$  are partly dispersed. The black tracks are for bodies that would be still associated with the observed Massalia family at the nominal HCM velocity cutoff  $V_c = 44$  m/s; the grey sections correspond to a configuration, when the body ceases to be HCM-associated with the nominal family. Some 16% of bodies leaked from the family via this process in our simulation.

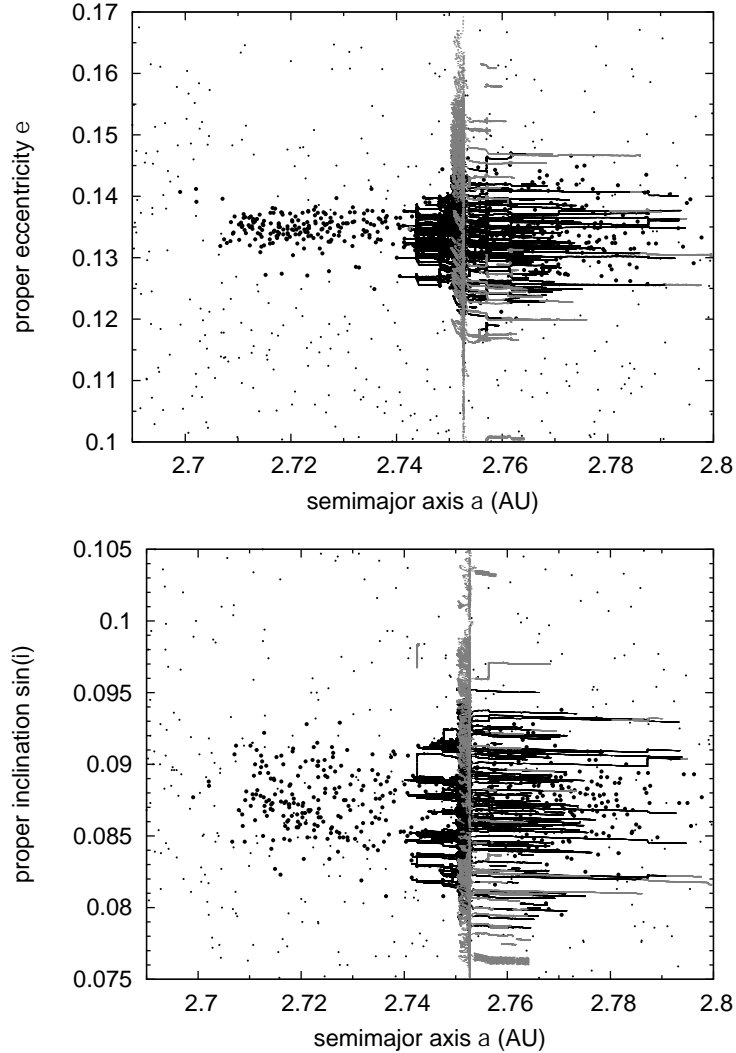


Fig. 25.— Evolution tracks of a sample of numerically integrated orbits with Yarkovsky forces in the Merxia family: (i) proper semimajor axis  $a$  vs proper eccentricity  $e$  (top), and (ii) proper semimajor axis  $a$  vs proper sine of inclination  $\sin I$  (bottom). Initial data of 145 selected real members, and their close clones, chosen near the center of the family. Obliquities, roughly set to  $45^\circ$ , make the bodies migrate toward larger values of the semimajor axis. Upon reaching the position of the three-body  $3J-1S-1$  resonance the proper  $e$  and proper  $\sin I$  are partly dispersed. The black tracks are for bodies that would be still associated with the observed Massalia family at the nominal HCM velocity cutoff  $V_c = 80$  m/s; the grey sections correspond to a configuration, when the body ceases to be HCM-associated with the nominal family. After crossing the resonance, the proper  $e$  and proper  $\sin I$  dispersion in the family increases to a level compatible with the observed members.

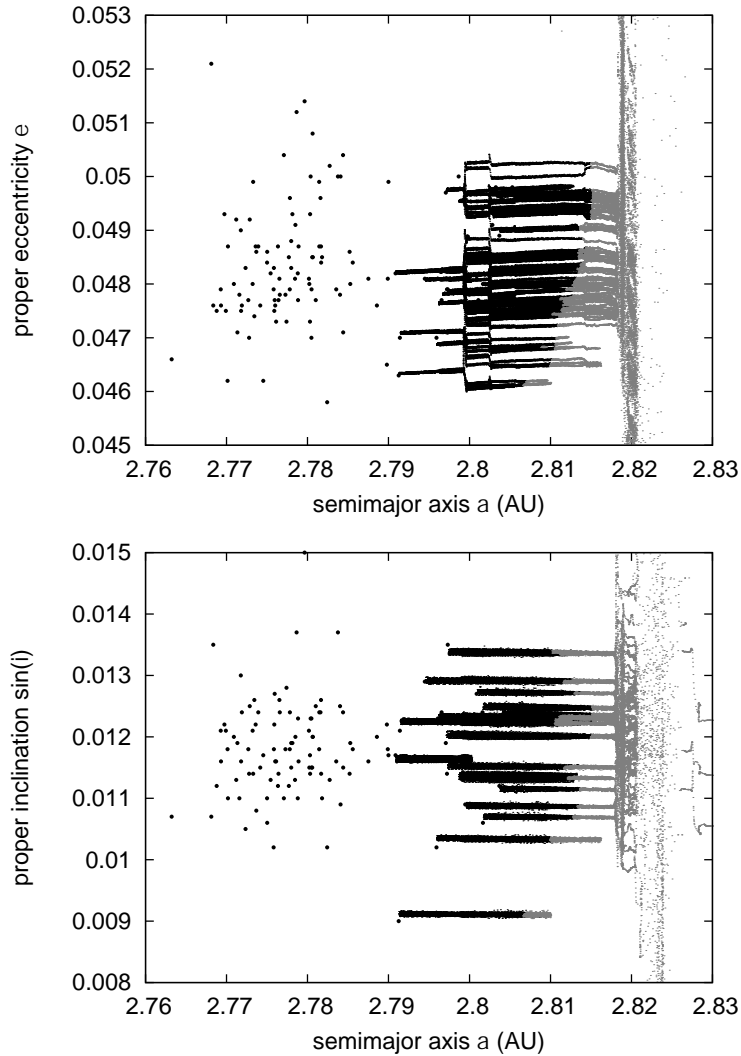


Fig. 26.— Evolution tracks of a sample of numerically integrated orbits with Yarkovsky forces in the Astrid family: (i) proper semimajor axis  $a$  vs proper eccentricity  $e$  (top), and (ii) proper semimajor axis  $a$  vs proper sine of inclination  $\sin(i)$  (bottom). Initial data of 110 selected real members, and their close clones, chosen near the center of the family. Obliquities, roughly set to  $45^\circ$ , make the bodies migrate toward larger values of the semimajor axis. The orbits continue quietly migrating until they reach separatrix of the J5/2 mean motion resonance with Jupiter where they are eliminated. At this level of sophistication, there is no sign why the zone between the observed Astrid family and the separatrix of the J5/2 should be prohibited; yet no asteroids –family or background– are observed in this zone.

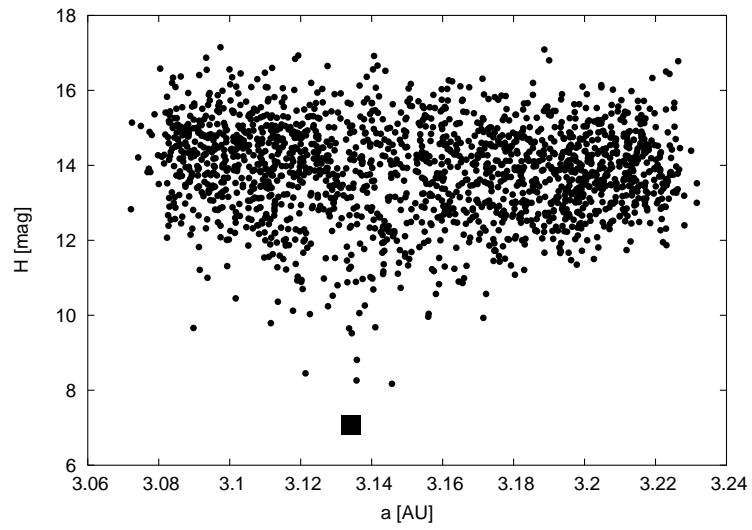


Fig. 27.— Themis family identified with the HCM cutoff velocity  $V_c = 58$  m/s projected onto a plane of proper semimajor axis  $a$  and absolute magnitude  $H$ . Filled square is (24) Themis.